

Model-based Bayesian inference of disease outbreak dynamics with invertible neural networks

An application to the COVID-19 pandemics in Germany

Stefan T. Radev, Frederik Graw, Simiao Chen, Nico T. Mutters,
Vanessa M. Eichel, Till Bärnighausen, and Ullrich Köthe

May 29, 2022

Abstract

Mathematical models in epidemiology strive to describe the dynamics and important characteristics of infectious diseases. Apart from their scientific merit, these models are often used to inform political decisions and interventional measures during an ongoing outbreak. Since high-fidelity models are often quite complex and analytically intractable, their applicability to real data depends on powerful estimation algorithms. Moreover, uncertainty quantification in such models is far from trivial, and different types of uncertainty are often confounded. With this work, we introduce a novel coupling between epidemiological models and specialized neural network architectures. This coupling results in a powerful Bayesian inference framework capable of principled uncertainty quantification and efficient amortized inference once the networks have been trained on simulations from an arbitrarily complex model. We illustrate the utility of our framework by applying it to real Covid-19 cases from entire Germany and German federal states.

1 Introduction

Epidemiological models are indispensable to plan and evaluate infection prevention and control (IPC) measures against infectious diseases. Moreover, epidemiological models can forecast the spread of a pandemic under different assumptions and thus allow to estimate the demand for medical hospital care and avoid potential shortages of medical equipment and capacities. In the case of communicable

diseases with immunity formation, these models typically take the form of systems of ordinary differential equations governing the transitions between different population compartments, such as, “Susceptible”, “Infected”, and “Recovered” (SIR) (see for example [1]). When various intrinsic properties of the disease (e.g., transmission rates and recovery periods) are known, SIR models and their extensions are successfully used to simulate outcomes of possible courses of action or non-action, that is, they solve the so-called *forward inference* problem. However, for newly arising infectious diseases such as Covid-19, these properties are initially unknown and must be estimated before realistic simulations can be performed. The estimation of hidden model parameters from observations of model outcomes is called *inverse inference* and constitutes a central task in many branches of science.

The inverse problem is also referred to as *model calibration* in the medical decision and health policy modeling literature [2]. The goal is to determine the values of the unknown model parameters such that the model outputs match the observed real-world data, the so-called *calibration targets*, as close as possible. Model calibration can be considered as an optimization problem seeking the best possible parameter configuration (e.g., by performing non-linear least squares minimization [3]). When the model’s outputs can be interpreted in a probabilistic manner, various maximum likelihood (ML) methods can also be applied. A disadvantage of most inference-as-optimization and ML methods is that they focus on accurate point estimation instead of principled uncertainty quantification. However, the latter is equally important when interpreting parameter values or making predictions about future outcomes.

An alternative but computationally more expensive approach is Bayesian model calibration using Markov chain Monte Carlo (MCMC) sampling to estimate the full posterior distribution of parameters given priors and observed data [4]. When the likelihood function is intractable or unknown, approximate Bayesian computation (ABC) can be used to approximate the posterior distribution of parameters [5, 6]. In contrast to optimization and ML approaches, Bayesian methods provide a principled way to quantify the epistemic uncertainty surrounding the inverse problem, because they return full posterior distributions rather than point estimates. Indeed, Bayesian inference with MCMC has been widely used in Covid-19 modeling studies [7, 8, 9]. Our approach aims to combine the advantages of optimization-based and Bayesian methods.

In particular, with this work we explore whether neural networks can facilitate model-based inverse inference in epidemiology. Our analysis on the basis of a novel neural network architecture called *BayesFlow* [10] answers this question in the affirmative. In contrast to mainstream neural network applications like image analysis, epidemiology poses two major challenges: (i) there are no

large training sets of annotated real-world data; and (ii) reliable uncertainty quantification of the network outputs is mandatory for these outputs to be usable in subsequent scenario simulations. Standard neural network architectures do not live up to these challenges.

We address these challenges in two ways: (i) We use networks that are specifically designed to perform Bayesian uncertainty quantification on their outputs. (ii) We leverage the epidemiological insight represented by SIR-type models by means of an alternative training procedure – *simulation-based training*. In our framework, a large number of plausible hypothetical scenarios – generated by a simulation program – is processed by the neural network until it becomes an expert in the interpretation of epidemiological observations. After completion of the training phase, the available real-world observations are passed to the network, which then estimates full Bayesian posterior distributions for the real-world parameters of interest. The ultimate goal of our approach is comparable to that of traditional simulation-based Bayesian inference methods, such as ABC, but our method operates much faster and generalizes to any real dataset within the scope of its training expertise [10].

During the initial outbreak of the Covid-19 pandemic, model-based inference was used to provide rapid estimates of key epidemiological parameters, which otherwise can be difficult to estimate directly from primary clinical tracing data. For instance, [11] incorporated domestic and international travel from and to Wuhan city in the SEIR model and used reported cases outside of Wuhan to infer the reproduction number R_0 and epidemic doubling time. The reproduction number of COVID-19 has been estimated using a similar approach in various settings [7][9]. In addition to estimating R_0 , [12] used an age-stratified SEIR model to infer age-specific mortality rates that corrected the biases due to the preferential ascertainment of severe cases and delayed mortality in Hubei China and Northern Italy. As another example, [13] estimated the reduction in the transmission rate by the implemented control measures in Wuhan using a SEIR model, which was further used to project the number of infections averted. Finally, [14] used a networked dynamic meta-population model to infer the fraction of undocumented infections and critical epidemiological characteristics. Importantly, since these SEIR-type models and extensions thereof are being used to forecast the dynamics of an epidemic with regard to public interventions or seasonal effects, reliable inference of key epidemiological parameters and trustworthy uncertainty quantification is paramount to support decision making.

We demonstrate the feasibility of our method by analyzing public Covid-19 data for Germany as a whole (three time-series: detected number of infected, recovered and deceased cases) and the German federal states individually (two time-series: detected number of infected and deceased cases). Since its first appearance in Wuhan in Dec 2019, the SARS-CoV-2 virus has infected more than 26 million people around the globe and caused more than 800,000 attributable deaths (up to 07 Sept

2020). Also Germany was severely affected by the pandemic, as around 250,000 people have been infected to date, from which almost 10,000 have been considered to have died as a consequence of the infection [15].

Our neural network is trained using simulations from a customized compartment model variant in combination with an observation model describing the differences between true and reported case numbers and an intervention model describing the IPC measures imposed by German authorities [16]. The full model has 34 unknown parameters in total and we express our prior knowledge about plausible parameter ranges by specifying relatively wide prior distributions and considering previous literature [16, 17].

After processing the reported data, our network estimates the joint posterior distribution of all model parameters. We observe that the posteriors are considerably narrower than the priors, that is, the network has gained a lot of additional information from the data. Credibility intervals of our parameter estimates are well in line with independently published results, and re-simulations starting at our estimated parameters fit the observed and future time-series very well. In particular, our inference suggests that approximately four fifths of all infectious individuals are undetected across all German federal states, which corresponds to the preliminary results of recent antibody studies and has profound implications for suggested relaxations of IPC measures.

2 Methods

2.1 Data Availability

The model was applied to epidemiological data on the number of reported Covid-19 cases (infected, recovered and deceased) in Germany and the individual federal states from March 01, 2020 until June 11, 2020. Data were obtained from publicly available sources. Code and scripts for reproducing all results and figures as well as for training new networks on new models are available at <https://github.com/stefanradev93/AIAgainstCorona>.

2.2 Neural Bayesian Parameter Estimation

The Bayesian perspective provides the mathematical tools and concepts for theoretically sound uncertainty-aware parameter estimation [4]. It requires prior knowledge about the nature of the forward process and reasonable parameter ranges as a starting point and combines it with information extracted from observed data into a *posterior distribution*, which represents our updated state of

knowledge. More formally, let θ be the vector of all hidden parameters and $X := x_{1:T} = [x_1, \dots, x_T]$ a multivariate epidemiological time-series. Then the well-known analytical formula for the posterior according to Bayes' rule is

$$p(\theta | X) = \frac{p(X | \theta) p(\theta)}{\int p(X | \theta) p(\theta) d\theta} \quad (1)$$

where $p(X | \theta)$ represents the forward model written as the likelihood of observing data X when the true parameters are θ , $p(\theta)$ is the prior distribution encoding our knowledge about plausible parameter combinations, and the denominator is a normalizing constant (the evidence).

Although conceptually simple, this formula poses two major challenges in the present setting: (i) Efficient and accurate approximation of the intractable posterior $p(\theta | X)$ is challenging. (ii) The likelihood is only implicitly defined via samples $x_{1:T} \sim p(X | \theta)$ created by repeatedly running the epidemiological simulation model. We solve both problems with our recently proposed neural Bayesian inference architecture (see [10] for full details). Its core component is an *invertible neural network* implemented as a *normalizing flow*. During the training phase, the invertible network is run in forward mode to learn an accurate model $q(\theta | X) \approx p(\theta | X)$ for the posterior distribution of parameters given any observation, using a large number of simulated pairs $(X_i, \theta_i) \sim p(X | \theta) p(\theta)$ as training data. In the inference phase, the network operates in the inverse direction (which is easy thanks to its invertible architecture) to estimate the posterior $q(\theta | X = x_{\text{obs}}) \approx p(\theta | X = x_{\text{obs}})$ for the *actually* observed data x_{obs} . Moreover, the network can be applied to multiple real observations without retraining, so that the training effort quickly amortizes over all inference queries (so called *amortized inference*). In addition, fast inverse inference facilitates model validation by making probabilistic calibration and posterior predictive checks on large validation datasets simple and very efficient [10].

2.3 The Epidemiological Model

In order to account for the specific nature of the current Covid-19 outbreak, our epidemiological model consists of three submodels: (i) a disease model describing the true dynamics of relevant population compartments; (ii) an intervention model describing the strengthening and relaxation of non-pharmaceutical counter-measures; and (iii) an observation model describing the deviations of published reports from the true values. These models build upon the previous work of [18, 16], who adapted the general SIR approach to the specifics of the Covid-19 epidemic and the situation in Germany. Parameter priors are based on our current state of knowledge about disease characteristics and government measures, but are chosen very wide to prevent them from dominating the information extracted from the actual observations.

Disease Model: The disease model is a system of non-linear ordinary differential equations (ODEs) comprising six compartments: susceptible (S), exposed (E - infected individuals who do not show symptoms and are not yet infectious), infected (I - symptomatic cases that are infectious), carrier (C - infectious individuals who recover without being detected), recovered (R), and dead (D), see figure 1a. Note that direct recovery from C covers all reasons why an infection might go undetected, that is, truly asymptomatic cases, lack of follow-up on pre-symptomatic cases, limited testing capacity under minor symptoms etc. are not differentiated by our model. Observations with limited accuracy (as described by the observation model below) are available for the compartments I, R, and D. The true time-series of all compartments are therefore considered latent and need to be estimated.

The ODEs for this SECIRD model read:

$$\frac{dS}{dt} = -\lambda(t) \left(\frac{C + \beta I}{N} \right) S \quad (2)$$

$$\frac{dE}{dt} = \lambda(t) \left(\frac{C + \beta I}{N} \right) S - \gamma E \quad (3)$$

$$\frac{dC}{dt} = \gamma E - (1 - \alpha) \eta C - \alpha \theta C \quad (4)$$

$$\frac{dI}{dt} = (1 - \alpha) \eta C - (1 - \delta) \mu I - \delta d I \quad (5)$$

$$\frac{dR}{dt} = \alpha \theta C + (1 - \delta) \mu I \quad (6)$$

$$\frac{dD}{dt} = \delta d I \quad (7)$$

The meaning of the model parameters and their priors are detailed in Table 1. Prior ranges are based on considerations in [16] and [17]. Note that the transmission rate $\lambda(t)$ is a function of time, because it is the parameter subjected to non-pharmaceutical interventions. In principle, changes in testing policy, medical advances etc. could also cause other parameters to become time-dependent, but this is not the case in the region and period considered in this paper.

Table 1: Description of disease model parameters and corresponding prior distributions

Parameter	Symbol	Prior Distribution
Number of initially exposed individuals	E_0	Gamma(2, 30)
Risk of infection from symptomatic patients	β	LogNormal(log(0.25), 0.3)
Rate at which exposed cases become infectious	γ	LogNormal(log(1/6.5), 0.5)
Rate at which symptoms manifest	η	LogNormal(log(1/3.2), 0.5)
Rate at which symptomatic individuals recover	μ	LogNormal(log(1/8), 0.2)
Rate at which undiagnosed individuals recover	θ	Uniform(1/14, 1/3)
Probability of remaining undetected/undiagnosed	α	Uniform(0.005, 0.99)
Rate at which critical cases die	d	Uniform(1/14, 1/3)
Probability of dying from the disease	δ	Uniform(0.01, 0.3)

Intervention Model: The intervention model controls the time-varying transmission rate $\lambda(t)$. Following [16], we define three change points encoding an assumed transmission rate reduction in response to IPC measures imposed by the German authorities. Each change point is represented by a piece-wise linear function with three degrees of freedom: the effect strength and the time interval for the effect to fully manifest itself. Their priors express the expected effect of each measure to reduce the transmission rate roughly by half after the date when it comes into force, but we leave very wide uncertainty margins to facilitate learning of the actual behavior. In addition, our model includes a fourth change point expressing the assumption that an eventual withdrawal of effective IPC measures (officially or due to non-compliance) will lead to a slight increase of the transmission rate. Prior distributions for all parameters are given in table Table 2. Note that we assume that interventions do not affect the risk of infection upon contact with a detected infectious individual (β).

Observation Model: The observation model represents the deviations between officially reported case counts and their true values. It comprises three error sources: the reporting delay, the weekly modulation (since testing and reporting activities are considerably reduced on weekends), and a noise term describing random fluctuations. Separate parameter sets are learned for each of the three publicly available time-series $I^{(obs)}$, $R^{(obs)}$, and $D^{(obs)}$ – the remaining compartments are considered unobservable. The relationship between the reported counts and their true values is described by the following set of discrete-time difference equations with time steps t measured in days. Note that the observed quantities only depend on the detectable symptomatic fraction of the infected population:

$$I_t^{(obs)} = I_{t-1}^{(obs)} + (1 - f_I(t)) (1 - \alpha) \eta C_{t-D_I} + \sqrt{I_{t-1}^{(obs)}} \sigma_I \xi_t \quad (8)$$

$$R_t^{(obs)} = R_{t-1}^{(obs)} + (1 - f_R(t)) (1 - \delta) \mu I_{t-D_R} + \sqrt{R_{t-1}^{(obs)}} \sigma_R \xi_t \quad (9)$$

$$D_t^{(obs)} = D_{t-1}^{(obs)} + (1 - f_D(t)) \delta d I_{t-D_D} + \sqrt{D_{t-1}^{(obs)}} \sigma_D \xi_t \quad (10)$$

where f_I, f_R, f_D represent the weekly modulation in reporting (with separate parameters for amplitude and phase as in [16]), D_I, D_R, D_D the reporting delays, and $\sigma_I, \sigma_R, \sigma_D$ the scales of multiplicative reporting noise, where the noise variables ξ_t follow a Student- t distribution with 4 degrees of freedom. The weekly modulation scalar f_E for each of the compartments $E \in \{I, R, D\}$ is computed as follows:

$$f_E(t) = (1 - A_E) \left(1 - \left| \sin \left(\frac{\pi}{7} t - 0.5 \Phi_E \right) \right| \right) \quad (11)$$

This yields three additional parameters for the weekly modulation amplitudes A_I, A_R, A_D , and phases Φ_I, Φ_R, Φ_D . Priors for the observation model's parameters are listed in Table 3.

Table 2: Description of intervention model parameters controlling the time-varying transmission rate

Parameter	Symbol	Prior Distribution
Onset date of each change to take effect	t_1	Normal(2020/03/09, 3)
	t_2	Normal(2020/03/16, 3)
	t_3	Normal(2020/03/23, 3)
	t_4	Normal(2020/05/06, 3)
Duration of each change to fully manifest itself	Δt_j	LogNormal(log(3), 0.3)
Transmission rates before / after each change	λ_0	LogNormal(log(1.2), 0.5)
	λ_1	LogNormal(log(0.6), 0.5)
	λ_2	LogNormal(log(0.3), 0.5)
	λ_3	LogNormal(log(0.1), 0.5)
	λ_4	LogNormal(log(0.15), 0.5)

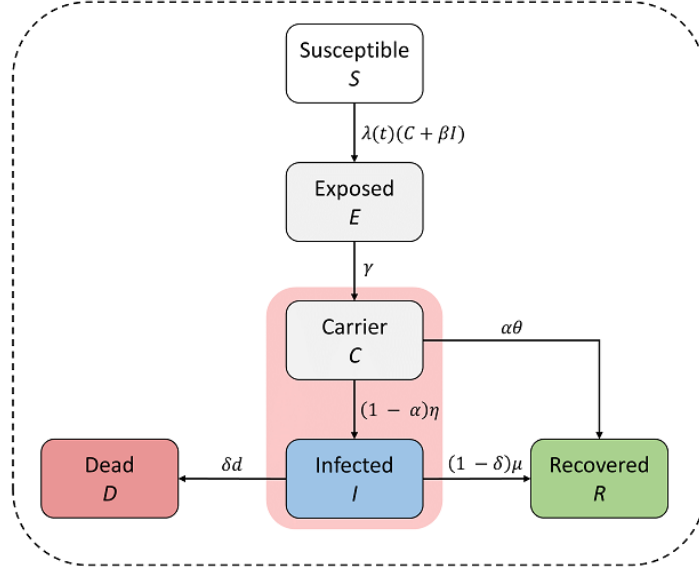
Table 3: Description of observation model parameters controlling properties of reporting

Parameter	Symbol	Prior Distribution
Reporting delays	D_I	LogNormal(log(8), 0.2)
	D_R	LogNormal(log(8), 0.2)
	D_D	LogNormal(log(8), 0.2)
Weekly modulation amplitudes	A_I	Beta(0.7, 0.17)
	A_R	Beta(0.7, 0.17)
	A_D	Beta(0.7, 0.17)
Weekly modulation phases	Φ_I	vonMises(0.01)
	Φ_R	vonMises(0.01)
	Φ_D	vonMises(0.01)
Reporting noise scale	σ_I	Gamma(1, 5)
	σ_R	Gamma(1, 5)
	σ_D	Gamma(1, 5)

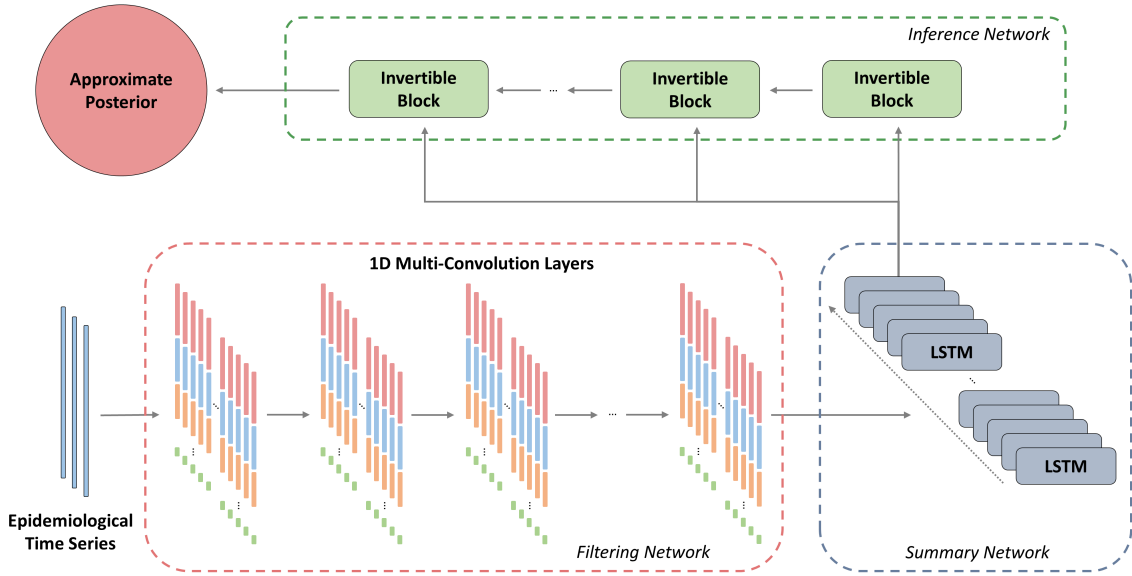
2.4 The BayesFlow Network for Epidemiological Inference

Our neural architecture comprises three subnetworks: (i) a convolutional *filtering* network performing noise reduction and feature extraction on the raw observational data; (ii) a recurrent *summary* network reducing preprocessed time-series of *varying* length to statistical summaries of *fixed* size; (iii) an invertible *inference* network performing Bayesian parameter inference, given the summary statistics of the observations. Figure 1b depicts the architecture of this composite network.

The design of the convolutional network is inspired by that of the Inception network which has shown tremendous success in computer vision tasks [19]. In particular, our network is implemented as a deep fully convolutional network which applies adjustable one-dimensional filters of different size at each level (cf. Figure 1b). The intuition behind this design is that filters of different size might capture patterns at different temporal scales (e.g., a filter of size one will capture daily fluctuations whereas a filter of size seven will capture weekly dynamics). This, in turn, should ease the task of extracting informative temporal features for parameter estimation.



(a) The disease submodel of our epidemiological model



(b) Our proposed neural architecture for amortized Bayesian inference

Figure 1: (a) The deterministic transitions between population compartments in continuous time as implemented by our model; (b) Inference with our trained neural Bayesian inference architecture using epidemiological time-series data. First, the (noisy) observed time-series are fed through a convolutional filtering network which extracts relevant features by keeping the temporal dimension of the data. Then, a many-to-one recurrent summary network reduces the transformed time-series to a fixed-sized vector of maximally informative summary statistics. Finally, an inference network approximates the full joint posterior over the model’s parameters given the output of the summary network.

The output of the convolutional network is a multivariate sequence containing the filtered epidemiological time-series. In order to reduce the filtered sequence to a fixed-size vector, we pass it through a long-short term memory (LSTM) recurrent network. Importantly, the LSTM network can deal with sequences of varying length, which enables online learning (i.e., Bayesian updating when new epidemiological data becomes available) and makes the same inference network applicable to settings with different data availability. Compared to a fixed pooling operation (e.g., mean or max), our recurrent network performs a learnable pooling operation which respects the sequential probabilistic symmetry of the data. In this way, our inference architecture learns to filter and extract the most informative features from the noisy observations in an end-to-end manner, such that no manual and potentially suboptimal selection of hand-crafted data features is required from the user.

Finally, the inference network has the task of *inverting* the forward model given the information extracted by the convolutional and recurrent networks. The inference network is implemented as a deep invertible conditional coupling flow [20] (see also [10] for more details on the design of conditional coupling flows for inference). The invertible network has two modes of operation.

During training, it is only evaluated in the *forward direction* and encouraged via a suitable optimization criterion to transform the posterior into a simple base distribution (e.g., Gaussian) from which samples can be easily obtained. Thus, the inference network integrates information both from the prior and from the data-generating mechanism (i.e., the implicit likelihood).

During inference, the inference network is only evaluated in the *inverse direction* using conditional information from real observed data passed through the filtering and summary networks. The posterior is approximated by repeatedly sampling from the simple base distribution and applying the inverse of the forward transformation learned during the training phase. Importantly, this method recovers the true posterior under perfect convergence of the optimization method [10].

More formally, let us denote the functions represented by the three networks as a , b , and c . Then the filtering network determines a filtered time series $\tilde{x}_{1:T} = a(x_{1:T})$ from observed data $x_{1:T}$, where the number of time steps T may vary according to data availability. The summary network turns the output of the filtering network into fixed-size vectors $y = b(\tilde{x}_{1:T})$. Finally, the inference network generates samples $\hat{\theta} \sim q(\theta | x_{1:T})$ from the parameter posterior by computing $\hat{\theta} = c^{-1}(y, z)$ with normally distributed random vectors $z \sim \mathcal{N}(0, \mathbb{I})$. The parameters of all three networks are optimized jointly during the training phase. Denoting the vector of all trainable network parameters as ϕ , the

three networks solve the following optimization criterion

$$\hat{\phi} = \underset{\phi}{\operatorname{argmin}} \mathbb{E}_{X \sim p(X)} [\mathbb{KL}(p(\theta | X) || q_{\phi}(\theta | X))] \quad (12)$$

$$= \underset{\phi}{\operatorname{argmin}} \mathbb{E}_{(X, \theta) \sim p(X, \theta)} [-\log q_{\phi}(\theta | X)] \quad (13)$$

We approximate the latter expectation via its empirical mean over samples $X, \theta \sim p(\theta, X)$ obtained via simulations from the forward model (see section 2.3).

As previously mentioned, one of the most important advantages of our method is *amortized inference*, owing to the fact that we approximate the posterior *globally* via a single set of network parameters $\hat{\phi}$. This is especially advantageous in epidemiological contexts, where the same model is applied in multiple populations (countries, cultures) or at different scales (states, regions), since the same pre-trained model can be repeatedly utilized for different populations and scales. Indeed, in the following real-world application, we demonstrate efficient amortized inference and excellent predictive performance with a single architecture applied simultaneously to epidemiological data from all German federal states.

2.5 Outbreak Prediction on the Basis of Estimated Posteriors

In a Bayesian context, posterior predictions can be derived from parameter estimates either for the purpose of model checking or for actual forecasts about future outcomes. Given observed timeseries $X := x_{1:t}$, the posterior predictive distribution for upcoming data $X' := x_{t+1:T}$ is given by:

$$p(X' | X) = \int p(X' | \theta, X) p(\theta | X) d\theta \quad (14)$$

This quantity is hard to compute, since it requires integration over the posterior. Moreover, it requires a numerical evaluation of the likelihood $p(X' | \theta, X)$, which in our case is not available in closed form. However, as mentioned previously, we approximate the posterior via samples $\{\theta^{(l)} \sim p(\theta | X)\}_{l=1}^L$. Note that the $\theta^{(l)}$ are drawn from the joint posterior, so that statistical dependencies and correlations between parameters are properly taken into account. Since we also have access to the simulator, we can obtain predictions by running the simulator with each posterior sample to obtain L simulated time-series $\{\tilde{X}^{(l)}\}_{l=1}^L$. We can then use these timeseries to obtain point predictions (e.g., by computing the mean or median for each time point), or quantify uncertainty (e.g., by computing quantiles or standard deviation for each time point). In this way, we are not only able to perform posterior checking about how the model reproduces the observations it was fitted to, but also to predict how

an outbreak will unfold over a future time frame.

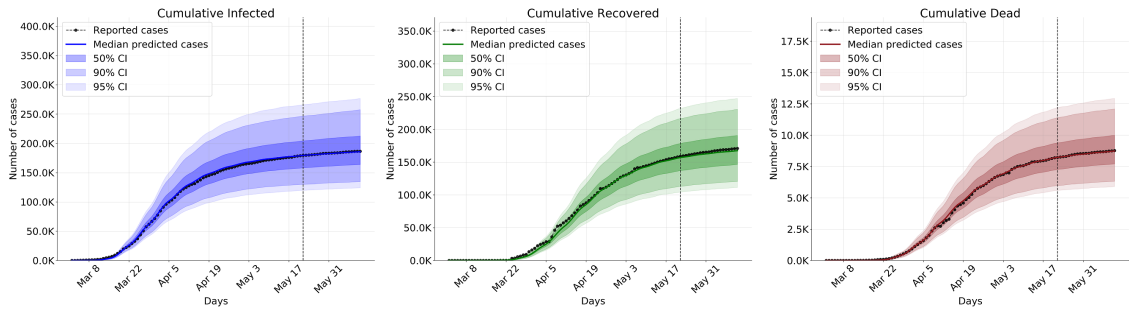
3 Results

3.1 Entire Germany

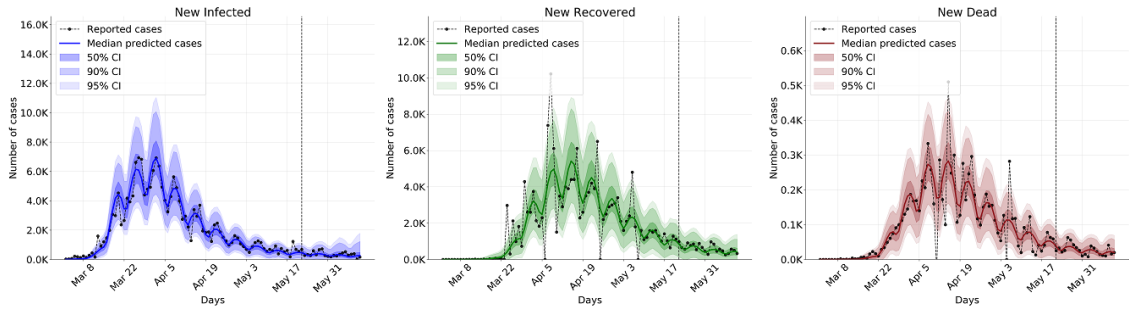
Full parameter posteriors and predictions obtained from entire Germany are depicted in Figure 2. First, utilizing the estimated joint posterior, our model yields good predictions and forecasts with well-calibrated uncertainty bounds for both cumulative (cf. Figure 2a) and new (cf. Figure 2b) infected, recovered, and diseased cases (see also Figure S1 for simulation-based probabilistic calibration of the approximate posteriors). Second, our parameter estimation results (cf. Figure 2c) are convergent with previous findings about central disease parameters [16]. Perhaps the most interesting results are those regarding the undetected diseased individuals. The median probability of remaining undetected (parameter α) lies at 0.63 and the maximum a posteriori (MAP) estimate at 0.79 (95%CI [0.07 – 0.91]). Notwithstanding the large uncertainty surrounding the number of undetected cases, the posterior of α is clearly far from uniform, and peaks well beyond 0.5 (see Figure 2c). This estimate is largely consistent with recent reports [21, 22, 23]. Additionally, our networks estimate a median number of 4.59 days (95%CI [2.99 – 11.11]) needed for undiagnosed (asymptomatic, weakly symptomatic etc.) individuals to recover (parameter $1/\theta$). In contrast, the median recovery rate of detected symptomatic individuals ($1/\mu$) is estimated at 8.06 days (95%CI [6.13 – 10.20]). Thus, the results support a general less severe disease progression for the undiagnosed individuals, since the latter recover faster [24]. Other central estimates are also in line with previous studies, for instance, the estimated rate at which symptoms manifest, η , (median 0.31, 95%CI [0.18 – 0.52]) has been reported to be around 0.25 according to [25] and between 0.16 and 0.2 according to the World Health Organization [26].

Finally, our results corroborate the timing of IPC measures and the gradual reduction in transmission rate observed in [16]. Furthermore, according to our estimates, the lifting of measures around May 6 would have led to approximately 40% increase in the transmission rate, as assumed by our prior. However, since the spreading rate at t_4 is already down to a median of 0.09 (95%CI: [0.05 – 0.15]), the increase to a median of 0.13 (95%CI [0.05 – 0.28]) does not lead to an exponential growth of infections.

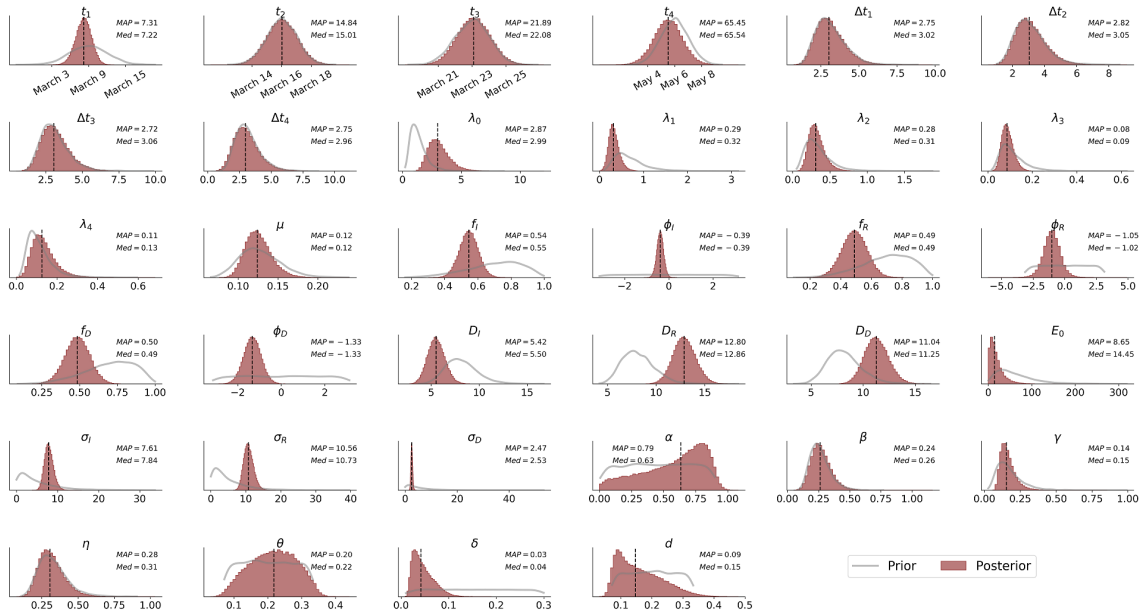
For completeness, Table 4 summarizes the estimated means, medians, MAPs, and 95%-CIs for all 34 model parameters.



(a) Model predictions of cumulative cases



(b) Model predictions of new cases



(c) Marginal parameter posteriors

Figure 2: (a) Posterior predictions and forecasts of cumulative cases obtained by inferring model parameters from data available from entire Germany. Cases to the left of the vertical dashed line were used for posterior checking (model fit) and cases to the right for posterior forecasts (predictions) on unseen data (b); Posterior predictions and forecasts on new cases; (c) Marginal posteriors of all 34 model parameters inferred from data from entire Germany alongside median and MAP summary statistics. Gray lines depict prior distributions for comparison with the posteriors. Vertical dashed lines indicate posterior medians.

Table 4: Posterior summaries and 95-%CIs for each model parameter inferred from data from entire Germany.

	Median	Mean	MAP	95-CI
t_1	7.222	7.198	7.350	[4.638 - 9.591]
t_2	15.004	15.007	14.970	[12.985 - 17.049]
t_3	22.088	22.098	21.944	[20.231 - 23.990]
t_4	65.531	65.528	65.482	[63.477 - 67.544]
Δt_1	3.016	3.139	2.786	[1.611 - 5.340]
Δt_2	3.045	3.161	2.872	[1.652 - 5.342]
Δt_3	3.059	3.177	2.835	[1.626 - 5.414]
Δt_4	2.947	3.075	2.722	[1.449 - 5.434]
λ_0	2.987	3.119	2.730	[1.704 - 5.310]
λ_1	0.320	0.336	0.292	[0.134 - 0.632]
λ_2	0.310	0.325	0.283	[0.157 - 0.582]
λ_3	0.087	0.090	0.080	[0.045 - 0.150]
λ_4	0.125	0.135	0.114	[0.047 - 0.277]
μ	0.124	0.126	0.121	[0.098 - 0.163]
f_I	0.545	0.545	0.540	[0.434 - 0.657]
ϕ_I	-0.390	-0.390	-0.400	[-0.687 - -0.092]
f_R	0.491	0.490	0.492	[0.326 - 0.648]
ϕ_R	-1.010	-1.015	-0.951	[-2.360 - 0.328]
f_D	0.486	0.485	0.490	[0.322 - 0.642]
ϕ_D	-1.333	-1.334	-1.291	[-2.129 - -0.552]
D_I	5.516	5.539	5.522	[3.874 - 7.348]
D_R	12.890	12.910	12.830	[10.728 - 15.212]
D_D	11.276	11.308	11.408	[9.149 - 13.651]
E_0	14.331	18.720	8.327	[1.195 - 61.374]
σ_I	7.843	7.916	7.634	[5.964 - 10.314]
σ_R	10.751	10.845	10.635	[8.364 - 13.882]
σ_D	2.527	2.544	2.501	[1.947 - 3.233]
α	0.632	0.579	0.793	[0.068 - 0.905]
β	0.263	0.271	0.246	[0.141 - 0.453]
γ	0.154	0.165	0.139	[0.092 - 0.302]
η	0.307	0.318	0.295	[0.178 - 0.521]
θ	0.218	0.216	0.243	[0.090 - 0.334]
δ	0.041	0.046	0.029	[0.018 - 0.097]
d	0.148	0.162	0.094	[0.067 - 0.321]

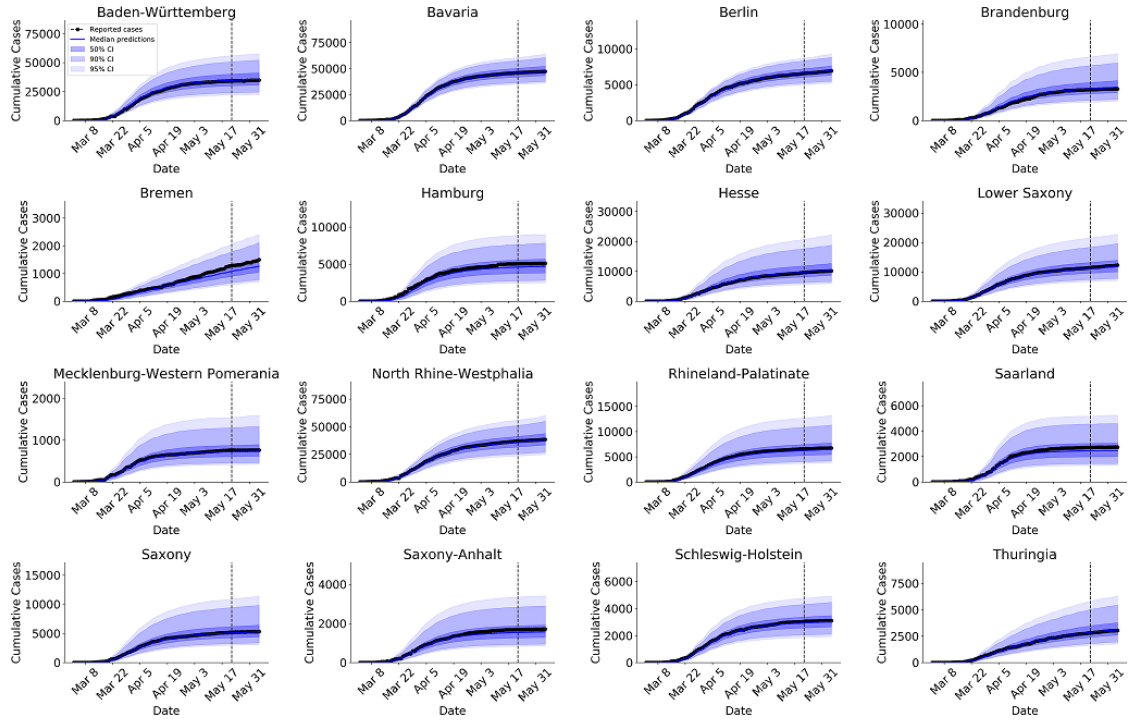


Figure 3: Model predictions of cumulative Covid-19 cases for each German federal state. Cases to the left of the vertical dashed line (8 weeks) were used for model fitting and posterior checking and cases to the right (3 weeks) for forecasts on new data. We observe that median model predictions closely match both past and future reported cases for each German federal state. Most importantly, the reported cases always lie within the estimated CIs, which vary across the federal states.

3.2 German Federal States

In the previous subsection, we demonstrated excellent model-based predictions and discussed parameter estimates obtained from epidemiological data from entire Germany. Here, we simulate epidemiological data from our custom model with varying population size N and train a *BayesFlow* network which we apply to epidemiological data from each German federal state. Training the network took approximately one day on a single GPU-machine, whereas obtaining posterior samples given data from all 16 states was nearly instant.

First, posterior predictions and forecasts for cumulative infections in each federal state are depicted in Figure 3 (see Figure S3 for predictions of cumulative deaths and Figure S2 for simulation-based probabilistic calibration of the approximate posteriors). Again, we observe that median predictions follow very closely the reported cumulative number of cases across all federal states. Furthermore, the reported cases are very well represented by the uncertainty bounds derived from the parameter posteriors, with prediction uncertainty growing as we move towards the future (cf. predictions after the dotted vertical lines in Figure 3). However, median predictions of cumulative deaths can become

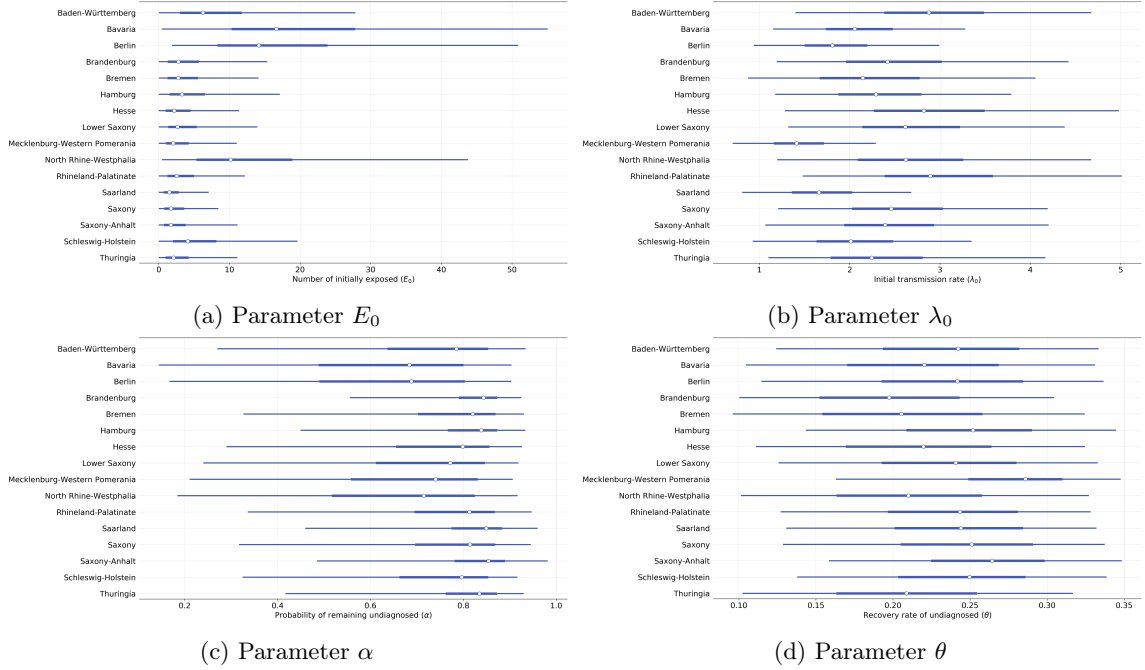


Figure 4: (a) Forest plot depicting 95% credibility intervals for the number of initially exposed individuals (E_0) obtained by amortized inference on data from all German federal states. Thin lines depict highest posterior density (HDI) intervals, thick lines depict posterior quartiles, and white points depict the corresponding medians of the estimated posteriors; (b) Initial transmission rate (λ_0); (c) Probability of remaining undiagnosed (α); (d) Recovery rate of undiagnosed (θ).

unreliable when only few cases are available (see predictions for the state Mecklenburg-Western Pomerania Figure S3), so well-calibrated uncertainty estimates are particularly important and need to be taken into account in addition to point predictions.

Second, full parameter posteriors recovered for each of the German federal states are depicted in the **Appendix**. Here, we will briefly focus on similarities/differences in four interesting latent parameters: probability of remaining undetected (α), recovery rate of undetected (θ), number of initially exposed individuals (E_0), and initial transmission rate (λ_0).

Posterior estimates of the parameters α and θ are depicted in Figure 4c and Figure 4d. First, we observe that posteriors of α across states tend to peak well above 0.5, suggesting that larger numbers of individuals have remained undetected/undiagnosed throughout the initial months of the Covid-19 pandemic in Germany. Further, there is a smaller probability to remain undiagnosed in the states of Bavaria, Berlin, and North Rhine-Westphalia than in other states. There are also some noticeable differences in the uncertainty surrounding α (compare for instance Brandenburg vs. Berlin). Second, there appears to be less interstate variability in the estimates of θ , suggesting an overall fast recovery of undiagnosed individuals.

In contrast, some interstate differences in the estimates of initially exposed individuals (E_0) are evident (cf. Figure 4a), with the states of Bavaria, Berlin, and North Rhine-Westphalia having pronouncedly more initially exposed individuals at onset than other states. Finally, Figure 4b depicts an interstate comparison between initial transmission rates. We observe that estimates vary between a median value of 2.27 across states, with the state Mecklenburg-Western Pomerania having the lowest and the state Baden-Württemberg having the highest median transmission rate at onset.

4 Discussion

In this work, we presented a novel simulation-based Bayesian inference framework for complex epidemiological models. We directly demonstrated the utility of our method by applying it to publicly available data on reported infected, recovered, and deceased individuals in Germany. We discussed how substantive conclusions and forecasts can be derived from parameter posteriors and also how to easily validate the resulting posteriors. We also used our posterior estimates to estimate two crucial parameters related to the undetected fraction of infected individuals: the probability of being diagnosed with the disease and the number of days undiagnosed individuals remain infectious. Our estimates suggest that a considerable number of individuals might have gone undetected through the course of the Covid-19 outbreak in Germany, confirming previous studies [21, 22, 23]. Further, our posteriors suggest that there is considerable uncertainty surrounding this estimate when derived in a purely model-based manner. Moreover, different summary statistics (e.g., means, medians, MAPs) derived from non-symmetric posteriors offer slightly different conclusions, thus highlighting the need to consider the full posteriors and corresponding credibility intervals.

Our neural Bayesian inference architecture enables efficient simulation-based inference for key epidemiological parameters using any mathematical model able to simulate the spread of an epidemic. With standard SIR-type of models based on (stochastic) ordinary differential equations generally providing a coarse-grained view on the epidemic dynamics [1], more complex models accounting for heterogeneous social interactions, age-dependent effects, and/or spatial and temporal heterogeneity [27, 28, 29, 30] become more important to predict the progression of an epidemic or guide IPC measures [30, 16, 31]. Furthermore, given the general uncertainty in reported numbers for emerging infectious diseases, estimation methods also need to account for this uncertainty when providing parameter estimates and be able to efficiently incorporate incoming data.

We argue that our *BayesFlow* architecture for epidemiological data provides a general inference framework for complex epidemiological scenarios. For example, it allows to introduce more or different

compartments, split compartments into strata (e.g. age groups) and add motility information. Especially the latter would likely improve our estimates of λ at the onset of the epidemic, since many cases in Germany acquired the disease abroad. Unfortunately, the required data are very hard to come by, so we refrained from implementing this possibility in the present paper.

Moreover, our approach has two key advantages over standard Bayesian methods. First, it can flexibly deal with arbitrarily complex models and data structures, requiring no closed-form likelihoods or *ad hoc* distributional restrictions regarding the shape of the joint prior or posterior. Second, the *amortized inference* property allows efficient posterior sampling, simultaneous application to multiple data sets as well as efficient online-learning and validation, once the networks have been trained with sufficient amounts of simulated data.

These advantages are important, since they enable researchers to concentrate on formulating, testing, and validating high-fidelity models without worrying about estimation efficiency or analytical tractability. We therefore believe that our proposed architecture can facilitate uncertainty-aware inference with complex and realistic epidemiological models, potentially revealing crucial dynamic aspects of a spreading disease and informing IPC measures. Future developments include Bayesian model comparison, multilevel modeling with hierarchical priors and a systematic comparison between different neural inference architectures.

Acknowledgment

This research was supported by the Deutsche Forschungsgemeinschaft (DFG, German Research Foundation; grant number GRK 2277 "Statistical Modeling in Psychology"). We thank the COVID-19 Research Grants by Google Cloud for partial support of this work.

References

- [1] M. J. Keeling and P. Rohani, *Modeling infectious diseases in humans and animals*. Princeton University Press, 2011.
- [2] C. Y. Kong, P. M. McMahon, and G. S. Gazelle, "Calibration of disease simulation model using an engineering approach," *Value in health*, vol. 12, no. 4, pp. 521–529, 2009.
- [3] M. Martcheva, *An introduction to mathematical epidemiology*, vol. 61. Springer, 2015.
- [4] A. Gelman, J. B. Carlin, H. S. Stern, D. B. Dunson, A. Vehtari, and D. B. Rubin, *Bayesian data analysis*. CRC press, 2013.

- [5] A. Minter and R. Retkute, “Approximate bayesian computation for infectious disease modelling,” *Epidemics*, vol. 29, p. 100368, 2019.
- [6] N. A. Menzies, D. I. Soeteman, A. Pandya, and J. J. Kim, “Bayesian methods for calibrating health policy models: a tutorial,” *Pharmacoeconomics*, vol. 35, no. 6, pp. 613–624, 2017.
- [7] M. Chinazzi, J. T. Davis, M. Ajelli, C. Gioannini, M. Litvinova, S. Merler, A. P. y Piontti, K. Mu, L. Rossi, K. Sun, *et al.*, “The effect of travel restrictions on the spread of the 2019 novel coronavirus (covid-19) outbreak,” *Science*, vol. 368, no. 6489, pp. 395–400, 2020.
- [8] C. M. Peak, R. Kahn, Y. H. Grad, L. M. Childs, R. Li, M. Lipsitch, and C. O. Buckee, “Individual quarantine versus active monitoring of contacts for the mitigation of covid-19: a modelling study,” *The Lancet Infectious Diseases*, 2020.
- [9] A. J. Kucharski, T. W. Russell, C. Diamond, Y. Liu, J. Edmunds, S. Funk, R. M. Eggo, F. Sun, M. Jit, J. D. Munday, *et al.*, “Early dynamics of transmission and control of covid-19: a mathematical modelling study,” *The lancet infectious diseases*, 2020.
- [10] S. T. Radev, U. K. Mertens, A. Voss, L. Ardizzone, and U. Köthe, “Bayesflow: Learning complex stochastic models with invertible neural networks,” *arXiv preprint arXiv:2003.06281*, 2020.
- [11] J. T. Wu, K. Leung, and G. M. Leung, “Nowcasting and forecasting the potential domestic and international spread of the 2019-ncov outbreak originating in wuhan, china: a modelling study,” *The Lancet*, vol. 395, no. 10225, pp. 689–697, 2020.
- [12] A. Hauser, M. J. Counotte, C. C. Margossian, G. Konstantinoudis, N. Low, C. L. Althaus, and J. Riou, “Estimation of sars-cov-2 mortality during the early stages of an epidemic: a modelling study in hubei, china and northern italy,” *medRxiv*, 2020.
- [13] H. Tian, Y. Liu, Y. Li, C.-H. Wu, B. Chen, M. U. Kraemer, B. Li, J. Cai, B. Xu, Q. Yang, *et al.*, “An investigation of transmission control measures during the first 50 days of the covid-19 epidemic in china,” *Science*, vol. 368, no. 6491, pp. 638–642, 2020.
- [14] R. Li, S. Pei, B. Chen, Y. Song, T. Zhang, W. Yang, and J. Shaman, “Substantial undocumented infection facilitates the rapid dissemination of novel coronavirus (sars-cov-2),” *Science*, vol. 368, no. 6490, pp. 489–493, 2020.
- [15] E. Dong, H. Du, and L. Gardner, “An interactive web-based dashboard to track covid-19 in real time,” *The Lancet infectious diseases*, vol. 20, no. 5, pp. 533–534, 2020.

- [16] J. Dehning, J. Zierenberg, F. P. Spitzner, M. Wibral, J. P. Neto, M. Wilczek, and V. Priesemann, “Inferring change points in the spread of covid-19 reveals the effectiveness of interventions,” *Science*, 2020.
- [17] B. Tang, X. Wang, Q. Li, N. L. Bragazzi, S. Tang, Y. Xiao, and J. Wu, “Estimation of the transmission risk of the 2019-ncov and its implication for public health interventions,” *Journal of Clinical Medicine*, vol. 9, no. 2, p. 462, 2020.
- [18] S. Khailaie, T. Mitra, A. Bandyopadhyay, M. Schips, P. Mascheroni, P. Vanella, B. Lange, S. Binder, and M. Meyer-Hermann, “Estimate of the development of the epidemic reproduction number r_t from coronavirus sars-cov-2 case data and implications for political measures based on prognostics,” *medRxiv*, 2020.
- [19] C. Szegedy, W. Liu, Y. Jia, P. Sermanet, S. Reed, D. Anguelov, D. Erhan, V. Vanhoucke, and A. Rabinovich, “Going deeper with convolutions,” in *Proceedings of the IEEE conference on computer vision and pattern recognition*, pp. 1–9, 2015.
- [20] D. P. Kingma and P. Dhariwal, “Glow: Generative flow with invertible 1x1 convolutions,” in *Advances in neural information processing systems*, pp. 10215–10224, 2018.
- [21] M. Day, “Covid-19: four fifths of cases are asymptomatic, china figures indicate,” 2020.
- [22] D. P. Oran and E. J. Topol, “Prevalence of asymptomatic sars-cov-2 infection: A narrative review,” *Annals of Internal Medicine*, 2020.
- [23] P. Poletti, M. Tirani, D. Cereda, F. Trentini, G. Guzzetta, G. Sabatino, V. Marziano, A. Castrofino, F. Grosso, G. Del Castillo, *et al.*, “Probability of symptoms and critical disease after sars-cov-2 infection,” *arXiv preprint arXiv:2006.08471*, 2020.
- [24] Z. Gao, Y. Xu, C. Sun, X. Wang, Y. Guo, S. Qiu, and K. Ma, “A systematic review of asymptomatic infections with covid-19,” *Journal of Microbiology, Immunology and Infection*, 2020.
- [25] W.-j. Guan, Z.-y. Ni, Y. Hu, W.-h. Liang, C.-q. Ou, J.-x. He, L. Liu, H. Shan, C.-l. Lei, D. S. Hui, *et al.*, “Clinical characteristics of coronavirus disease 2019 in china,” *New England journal of medicine*, vol. 382, no. 18, pp. 1708–1720, 2020.
- [26] W. H. Organization *et al.*, “Report of the who-china joint mission on coronavirus disease 2019 (covid-19). 2020,” *Significant account of fatality rates and comorbidities in reports from China related to COVID-19 infection*, 2020.

- [27] R. A. Neher, R. Dyrda, V. Druelle, E. B. Hodcroft, and J. Albert, “Potential impact of seasonal forcing on a sars-cov-2 pandemic,” *Swiss medical weekly*, vol. 150, no. 1112, 2020.
- [28] R. E. Baker, W. Yang, G. A. Vecchi, C. J. E. Metcalf, and B. T. Grenfell, “Susceptible supply limits the role of climate in the early sars-cov-2 pandemic,” *Science*, 2020.
- [29] N. M. Ferguson, D. A. Cummings, C. Fraser, J. C. Cajka, P. C. Cooley, and D. S. Burke, “Strategies for mitigating an influenza pandemic,” *Nature*, vol. 442, no. 7101, pp. 448–452, 2006.
- [30] N. G. Davies, A. J. Kucharski, R. M. Eggo, A. Gimma, W. J. Edmunds, T. Jombart, K. O’Reilly, A. Endo, J. Hellewell, E. S. Nightingale, *et al.*, “Effects of non-pharmaceutical interventions on covid-19 cases, deaths, and demand for hospital services in the uk: a modelling study,” *The Lancet Public Health*, 2020.
- [31] S. Flaxman, S. Mishra, A. Gandy, H. J. T. Unwin, T. A. Mellan, H. Coupland, C. Whittaker, H. Zhu, T. Berah, J. W. Eaton, *et al.*, “Estimating the effects of non-pharmaceutical interventions on covid-19 in europe,” *Nature*, pp. 1–8, 2020.

Appendix

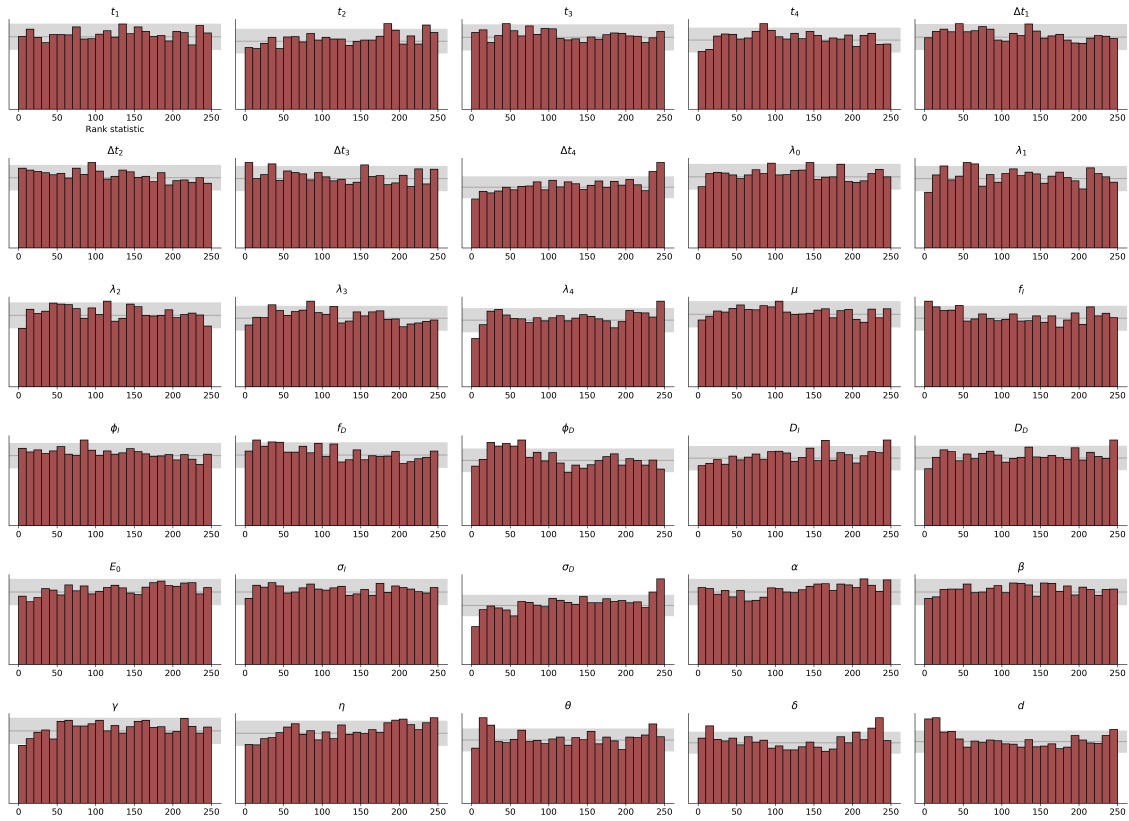


Figure S1: Simulation-based probabilistic calibration of the marginal approximate posteriors obtained by the network trained for inference on entire Germany. Uniformly distributed histograms of the rank statistic indicate no systematic biases in the estimation of location and scale of the true marginal posteriors.

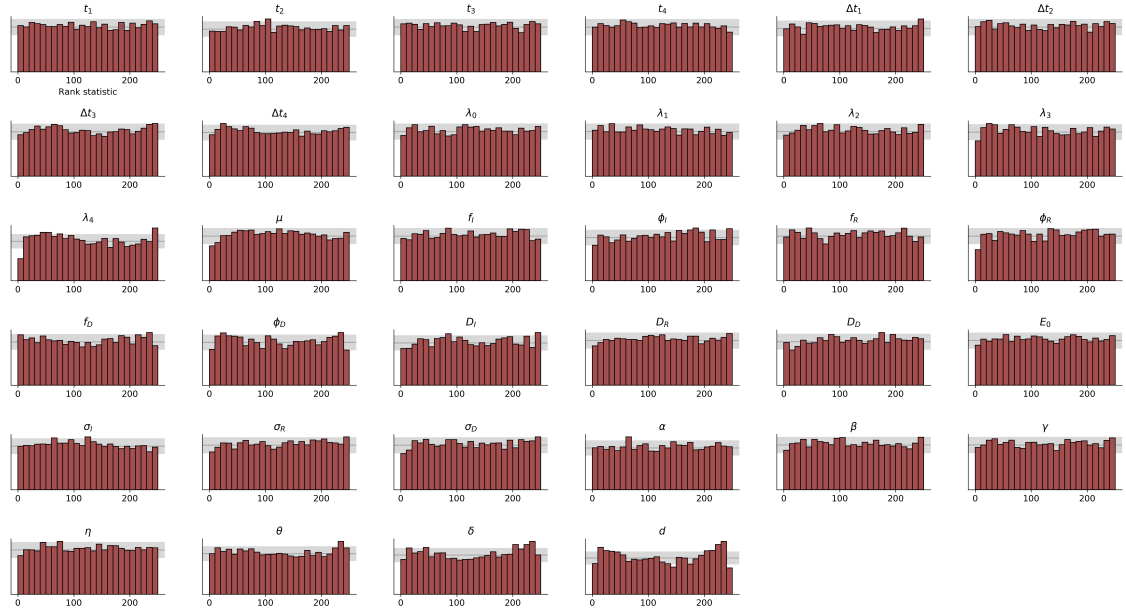


Figure S2: Simulation-based probabilistic calibration of the marginal approximate posteriors obtained by the networks trained for amortized inference on all German federal states. Uniformly distributed histograms of the rank statistic indicate no systematic biases in the estimation of location and scale of the true marginal posteriors.

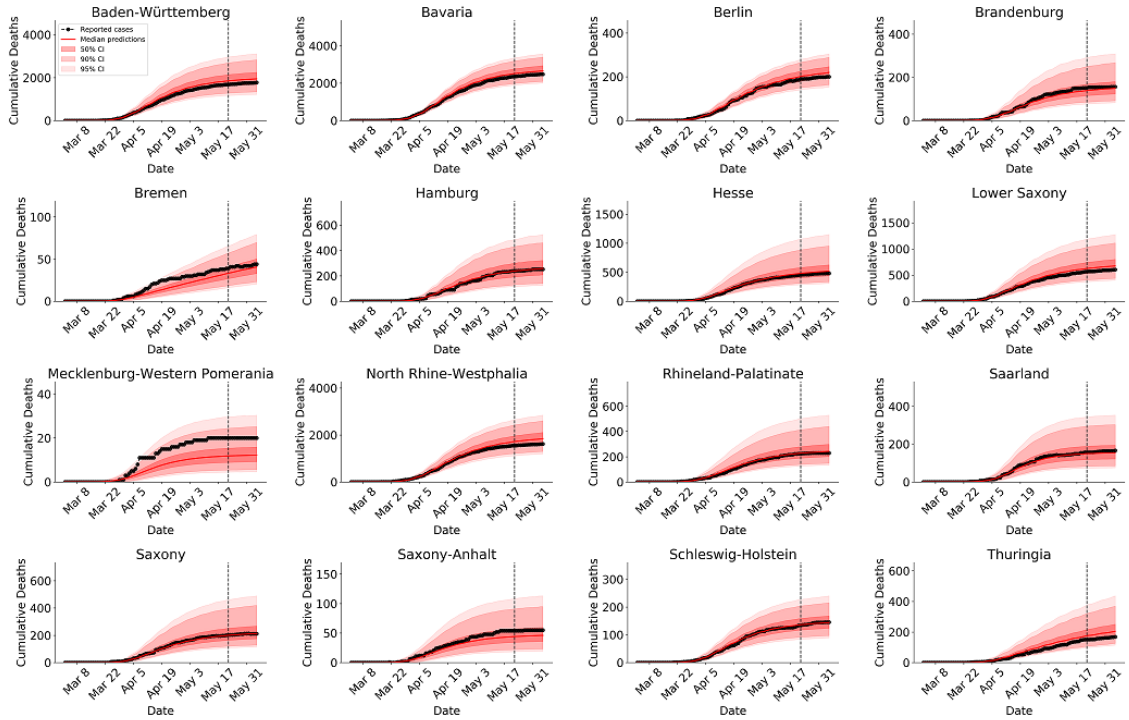


Figure S3: Model predictions of cumulative Covid-19 deaths for each German federal state. Cases to the left of the vertical dashed line (8 weeks) were used for model fitting and posterior checking and cases to the right (3 weeks) for forecasts on new data. We observe good matches between the model's median predictions and past and future reported cases for each German federal state. However, the number of deaths in the state Mecklenburg-Western Pomerania over time is underestimated (although it lies mostly within the estimated 95%-CI), which is probably due to the very low counts (lowest among all German federal states).

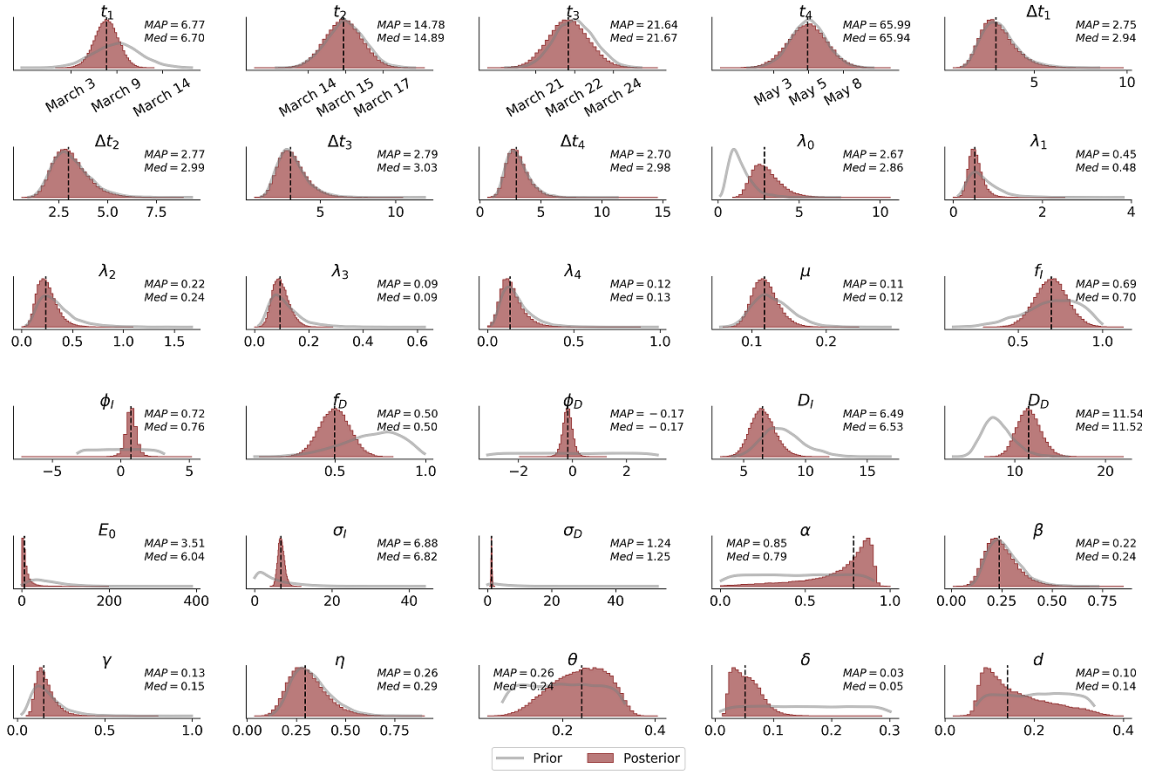


Figure S4: Marginal parameter posteriors from data available for the German federal state Baden-Württemberg.

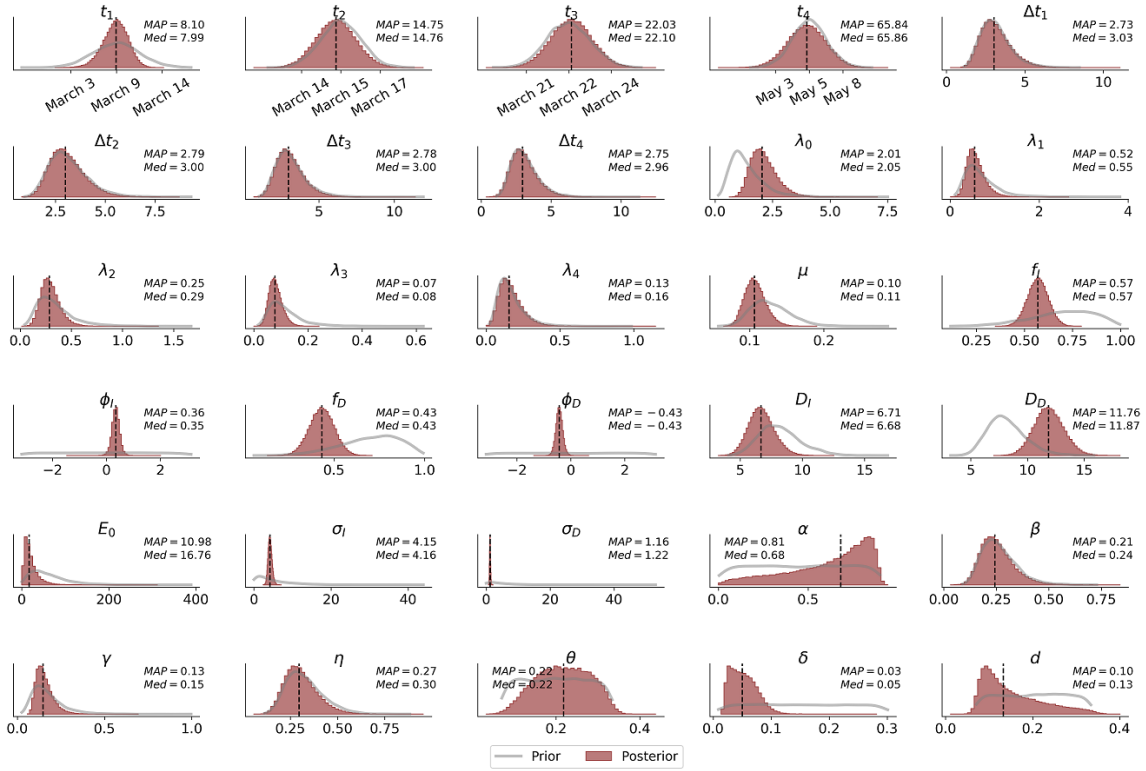


Figure S5: Marginal parameter posteriors from data available for the German federal state Bavaria.

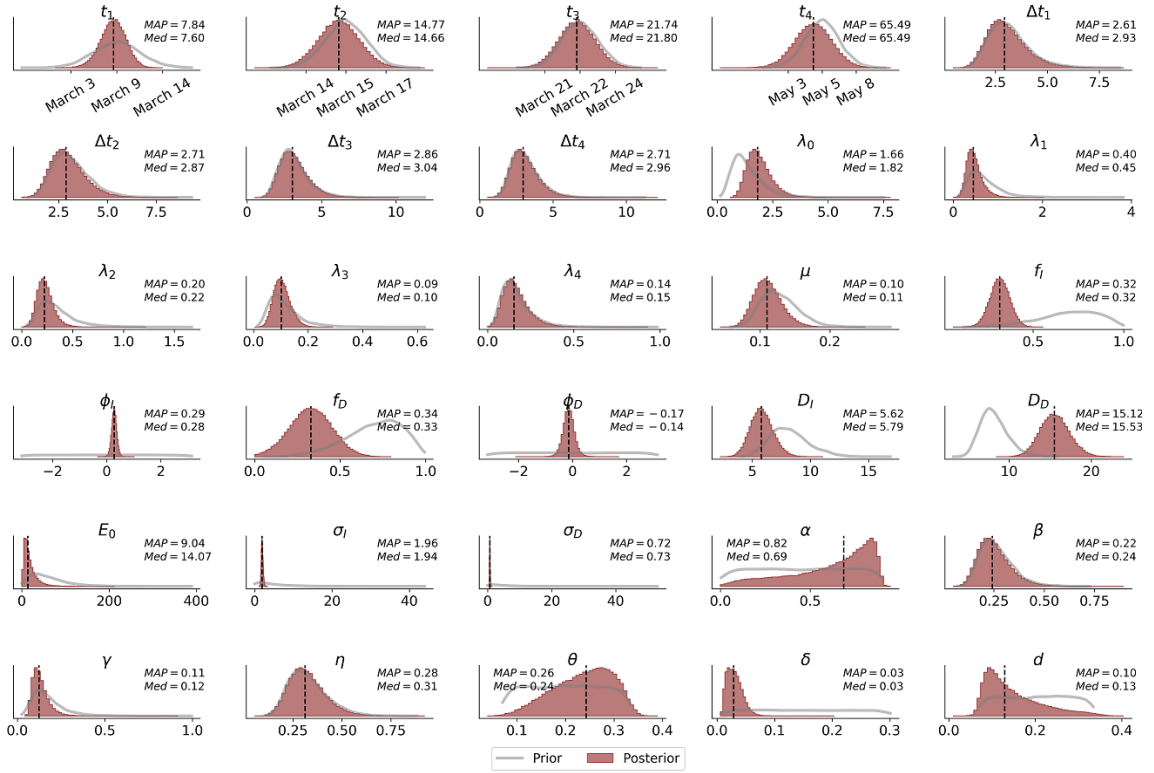


Figure S6: Marginal parameter posteriors from data available for the German federal state Berlin.

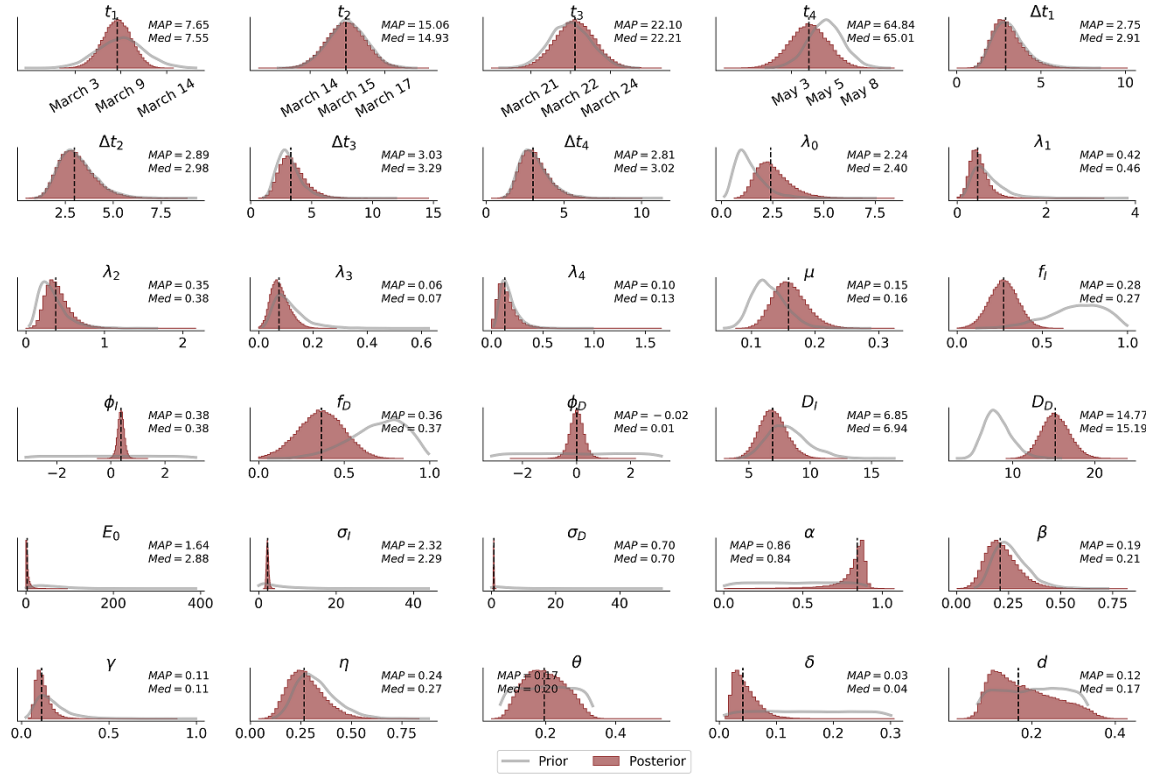


Figure S7: Marginal parameter posteriors from data available for the German federal state Brandenburg.

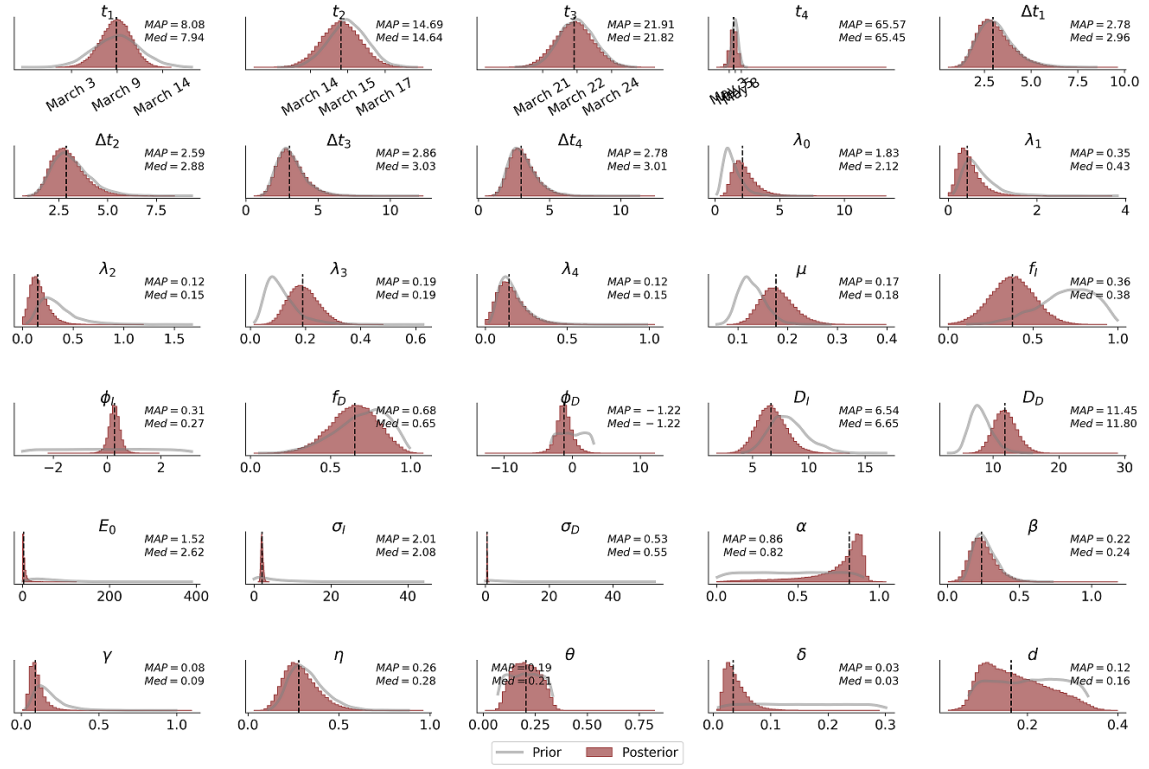


Figure S8: Marginal parameter posteriors from data available for the German federal state Bremen.

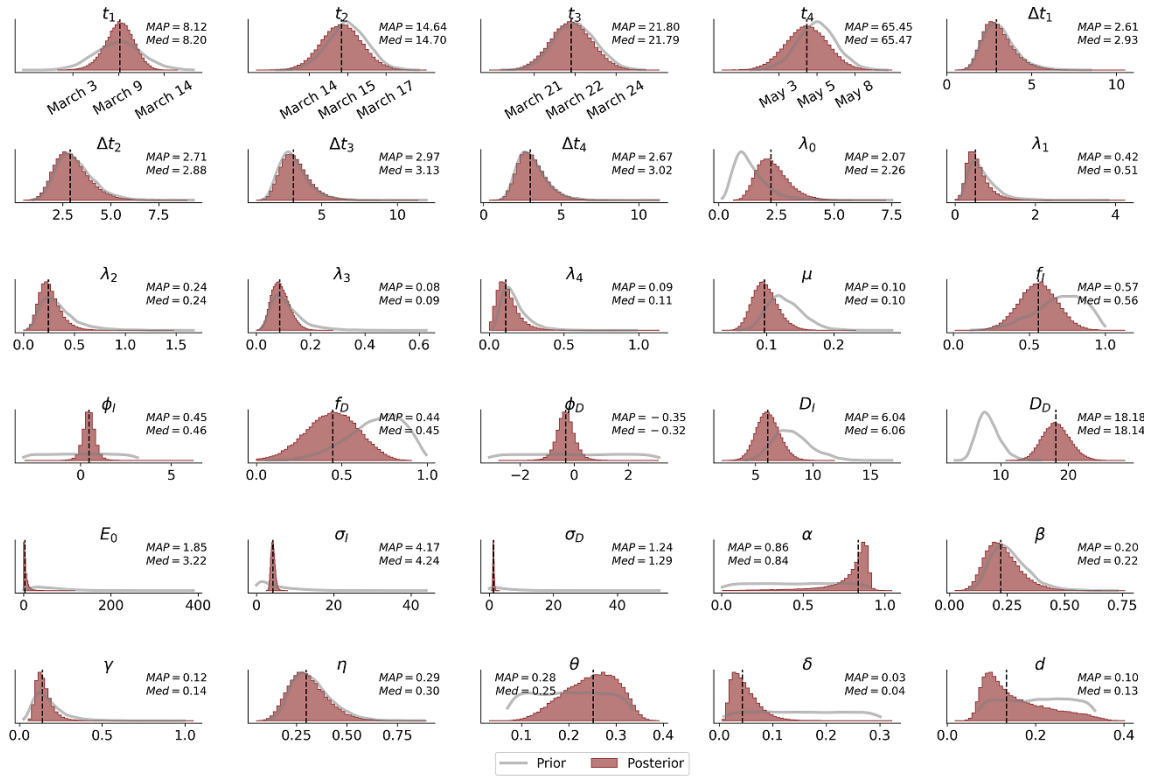


Figure S9: Marginal parameter posteriors from data available for the German federal state Hamburg.

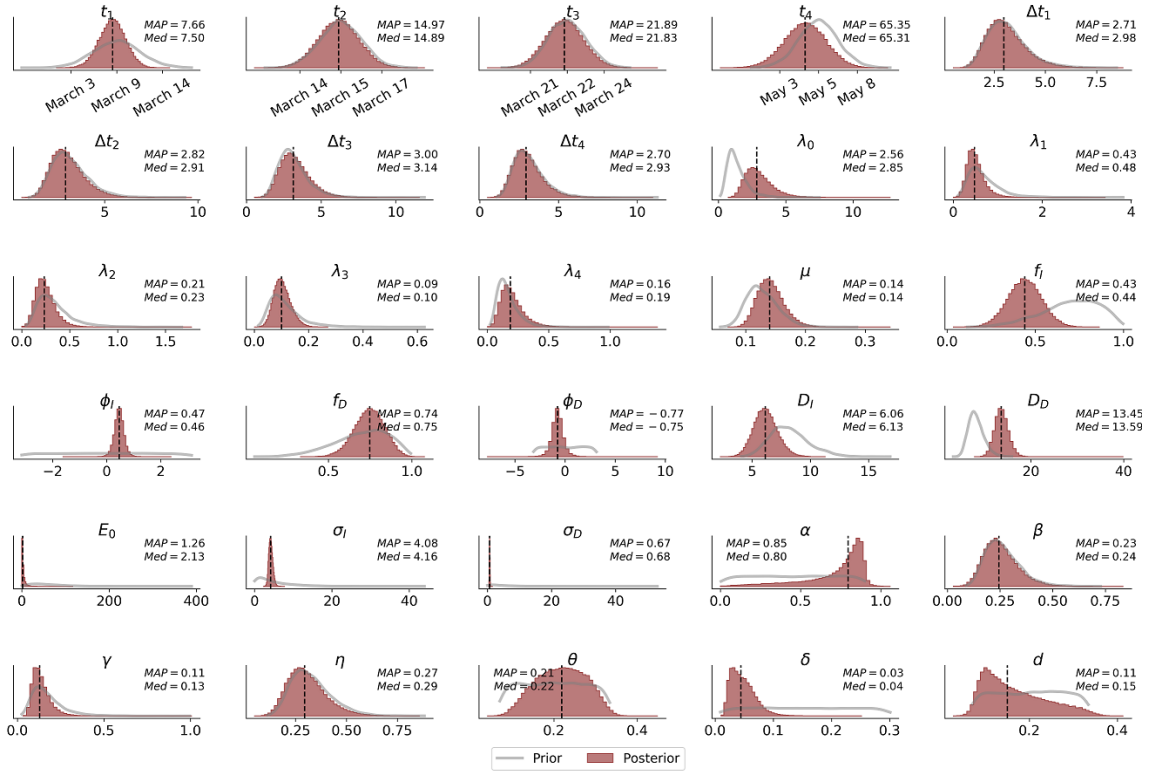


Figure S10: Marginal parameter posteriors from data available for the German federal state Hesse.

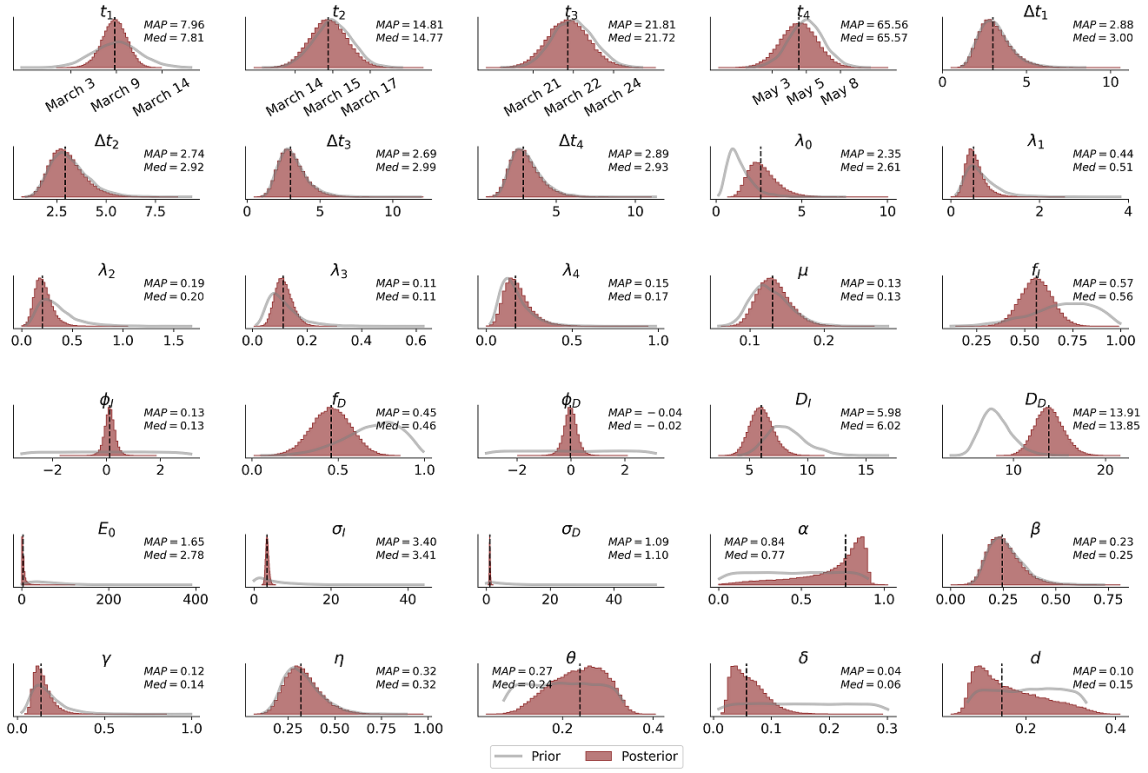


Figure S11: Marginal parameter posteriors from data available for the German federal state Lower Saxony.

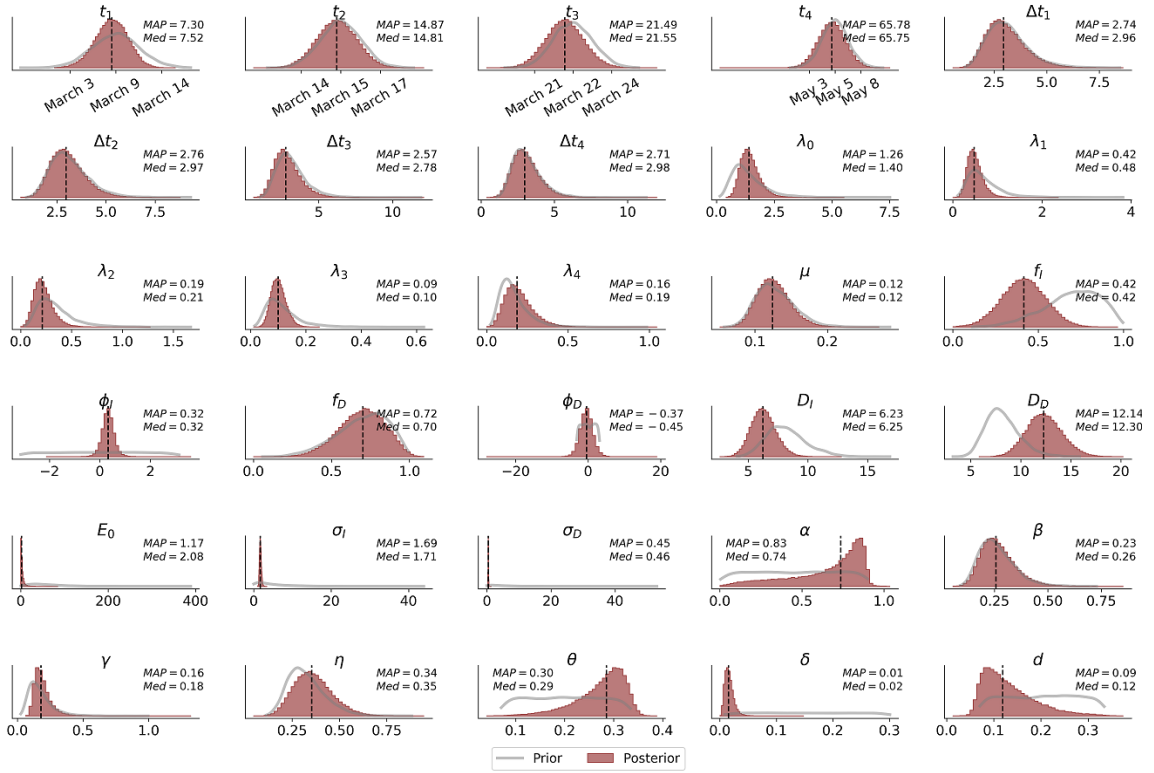


Figure S12: Marginal parameter posteriors from data available for the German federal state Mecklenburg-Western Pomerania.

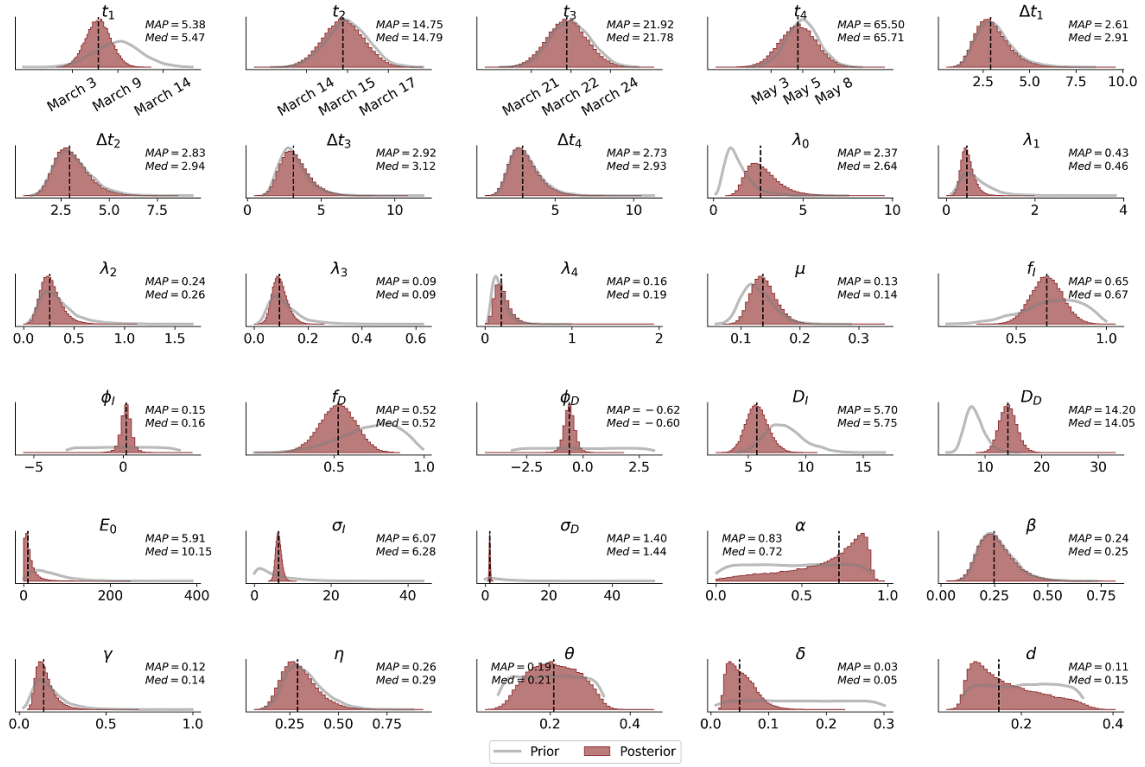


Figure S13: Marginal parameter posteriors from data available for the German federal state North Rhine-Westphalia.

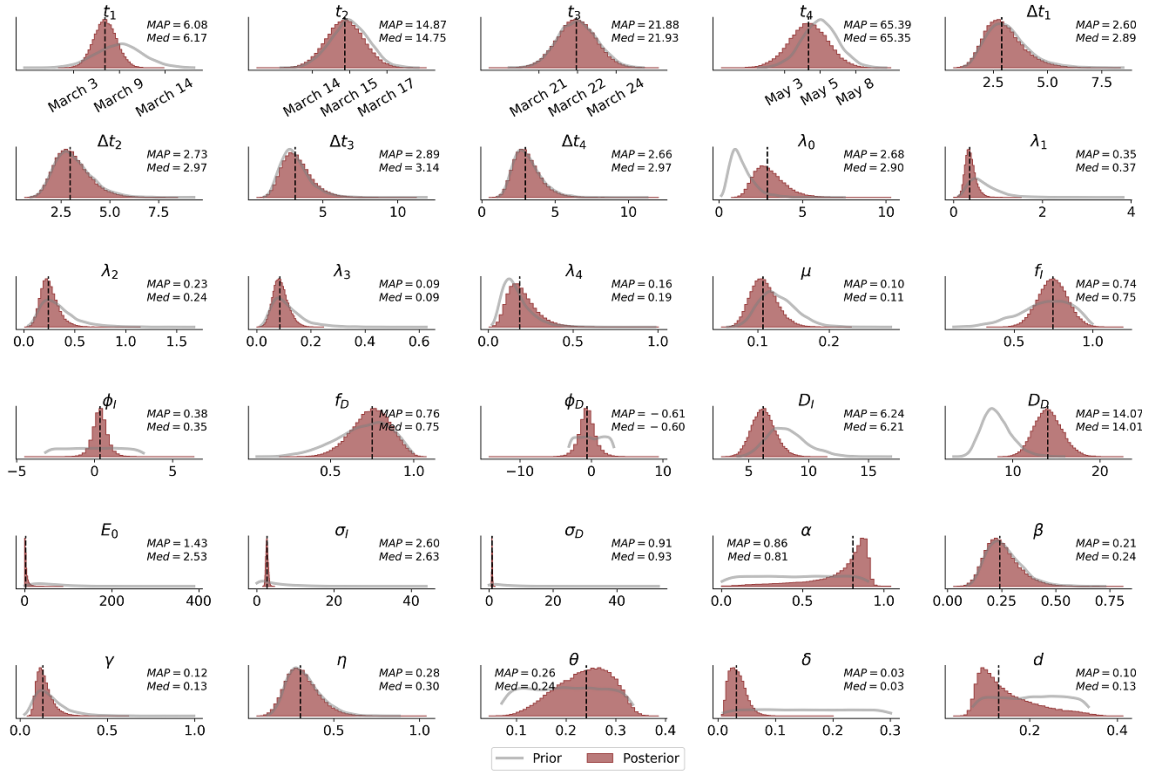


Figure S14: Marginal parameter posteriors from data available for the German federal state Rhineland-Palatinate.

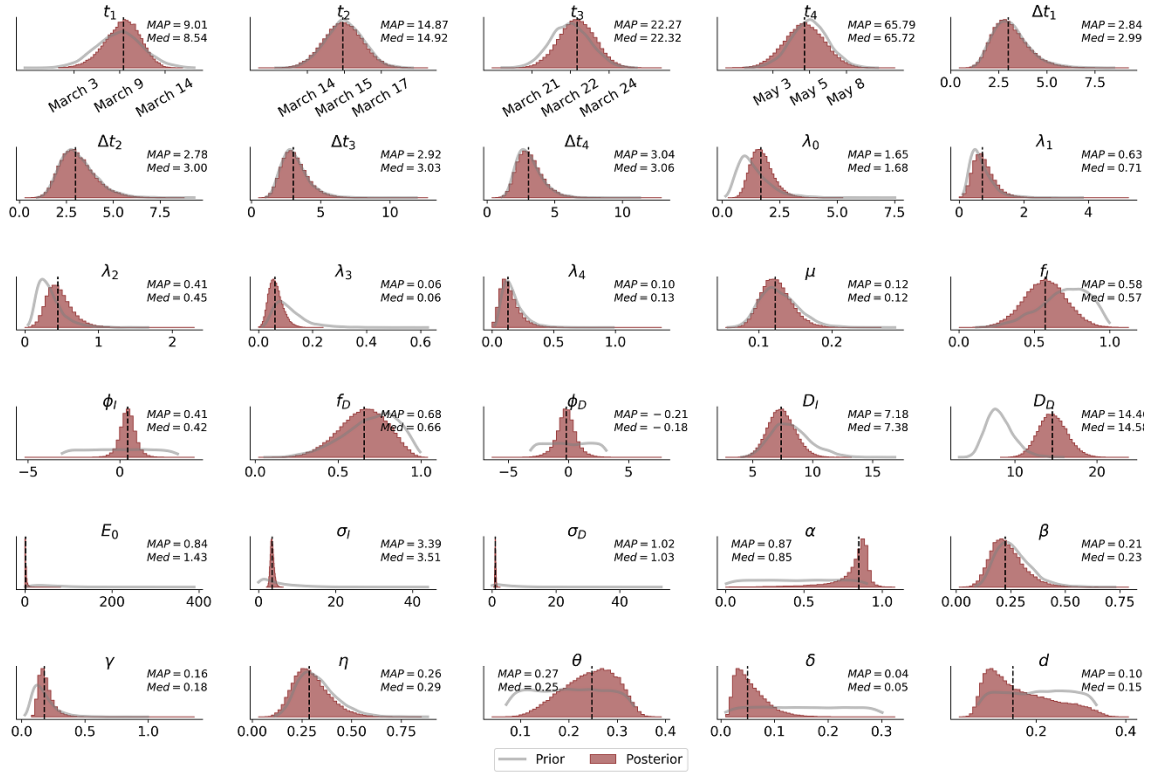


Figure S15: Marginal parameter posteriors from data available for the German federal state Saarland.

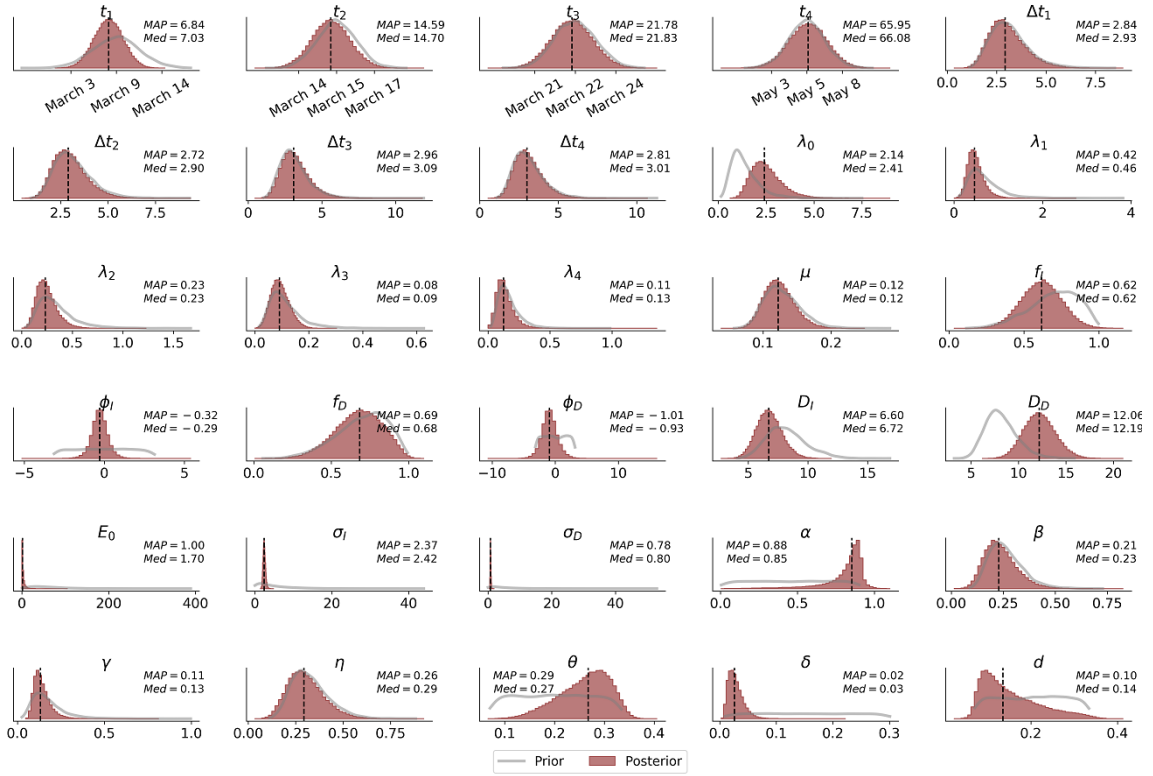


Figure S16: Marginal parameter posteriors from data available for the German federal state Saxony-Anhalt.

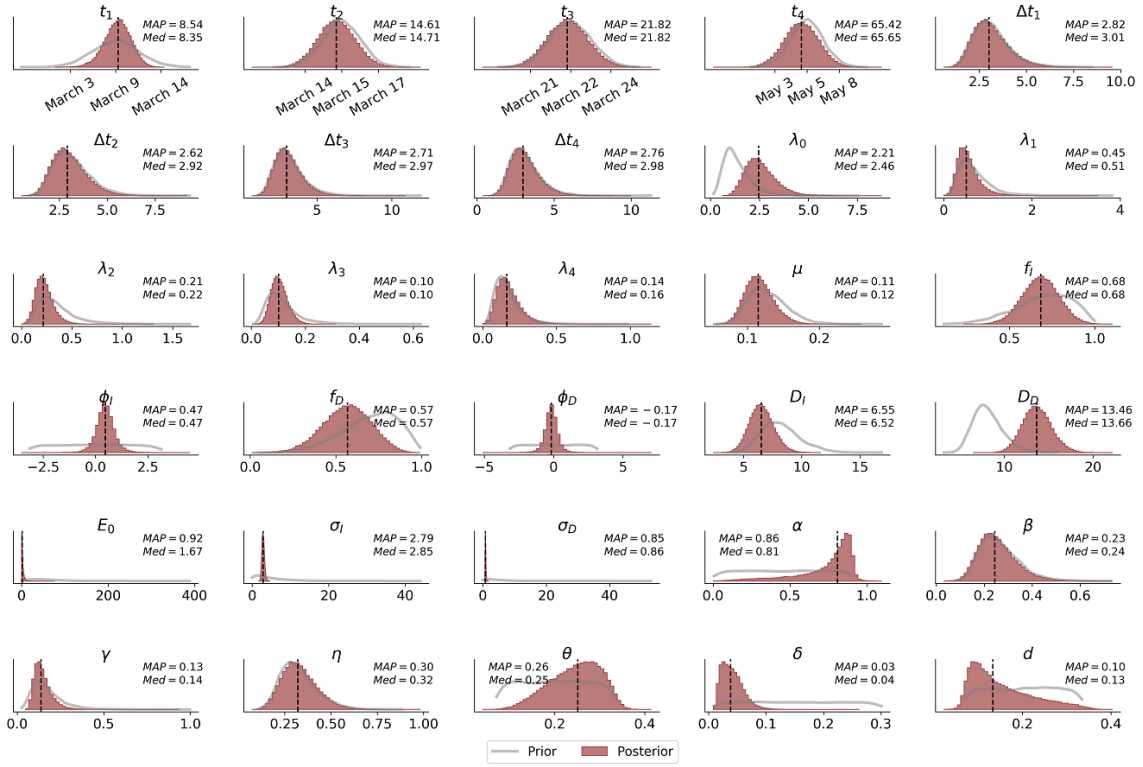


Figure S17: Marginal parameter posteriors from data available for the German federal state Saxony.

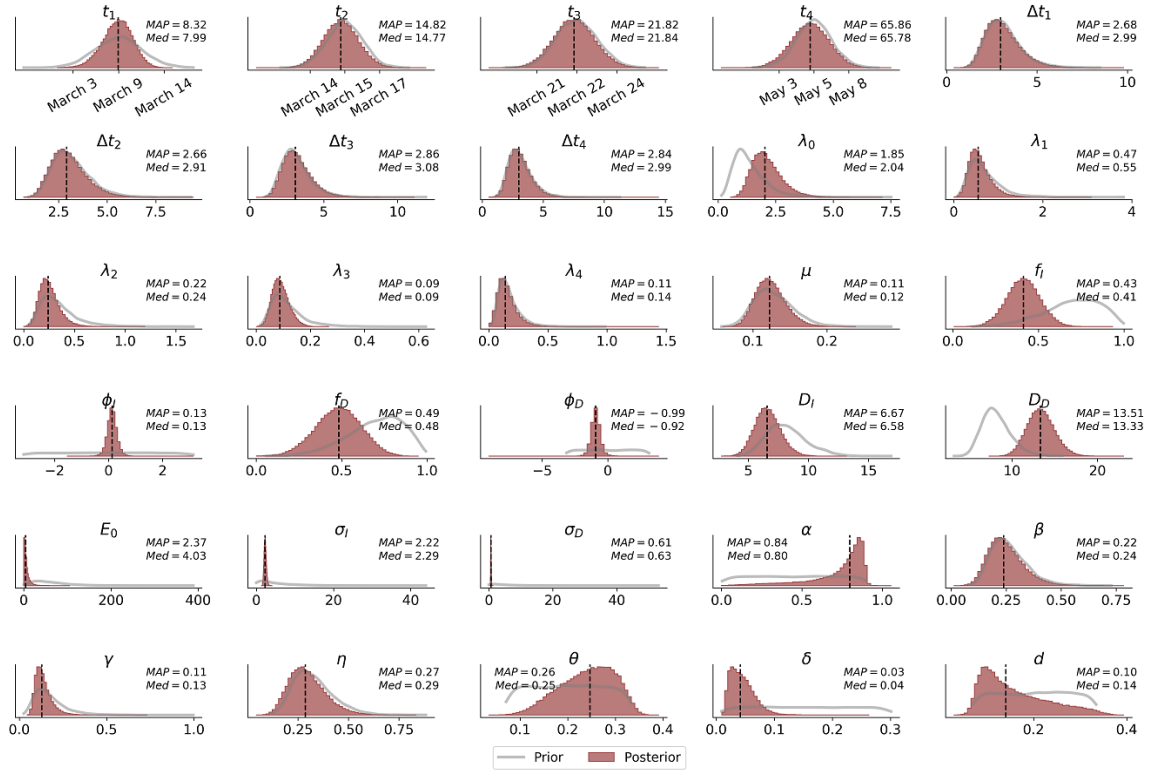


Figure S18: Marginal parameter posteriors from data available for the German federal state Schleswig-Holstein.

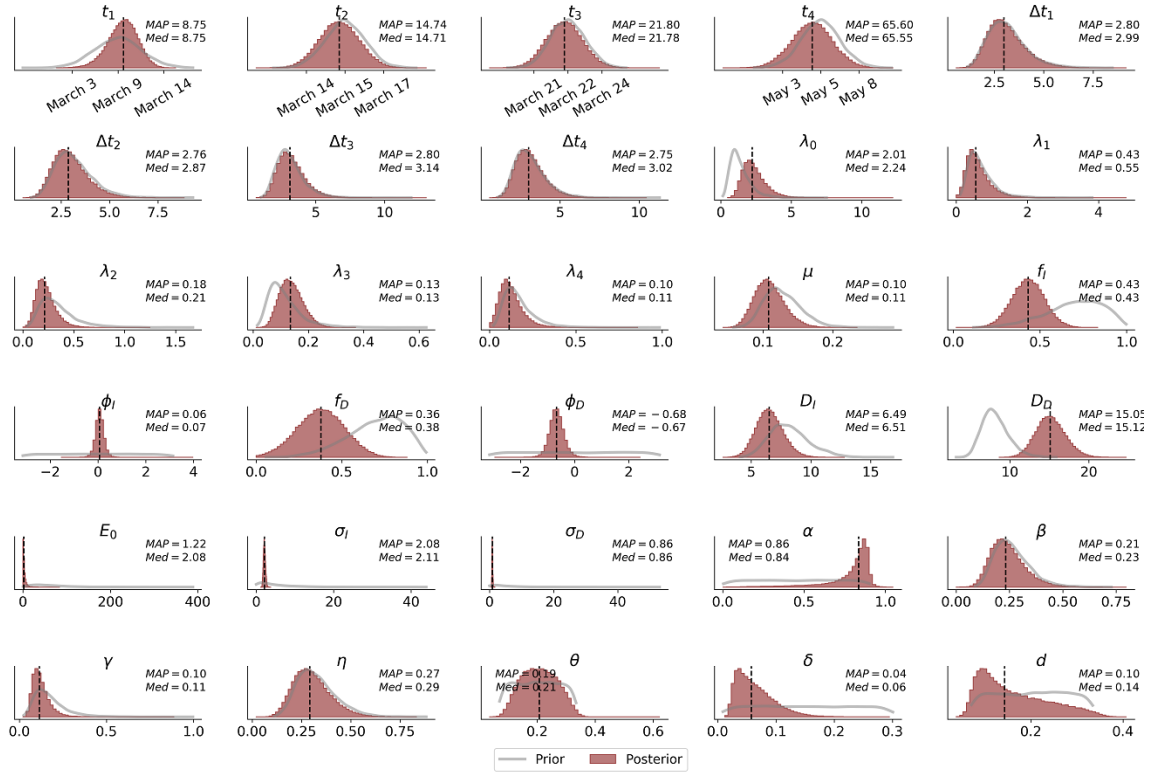


Figure S19: Marginal parameter posteriors from data available for the German federal state Thuringia.

Table S1: Posterior summaries and 95-% credibility intervals for each model parameter recovered from data from the German federal state Baden-Württemberg.

	Median	Mean	MAP	95-CI
t_1	6.706	6.683	6.898	[3.587 - 9.669]
t_2	14.885	14.881	14.929	[13.000 - 16.753]
t_3	21.668	21.680	21.615	[19.721 - 23.711]
t_4	65.951	65.945	66.064	[63.740 - 68.128]
Δt_1	2.948	3.068	2.723	[1.597 - 5.210]
Δt_2	2.988	3.097	2.688	[1.669 - 5.153]
Δt_3	3.030	3.153	2.880	[1.651 - 5.358]
Δt_4	2.982	3.108	2.875	[1.655 - 5.293]
λ_0	2.862	2.995	2.705	[1.622 - 5.145]
λ_1	0.483	0.504	0.453	[0.247 - 0.885]
λ_2	0.236	0.251	0.209	[0.097 - 0.490]
λ_3	0.094	0.097	0.086	[0.044 - 0.166]
λ_4	0.131	0.143	0.115	[0.043 - 0.312]
μ	0.117	0.118	0.115	[0.088 - 0.156]
f_I	0.696	0.696	0.715	[0.506 - 0.884]
ϕ_I	0.759	0.758	0.771	[-0.047 - 1.559]
f_D	0.497	0.496	0.504	[0.329 - 0.657]
ϕ_D	-0.174	-0.173	-0.186	[-0.541 - 0.197]
D_I	6.534	6.581	6.438	[4.746 - 8.672]
D_D	11.520	11.570	11.522	[9.146 - 14.278]
E_0	6.017	9.409	3.464	[0.570 - 38.363]
σ_I	6.818	6.880	6.578	[5.397 - 8.708]
σ_D	1.246	1.256	1.205	[0.963 - 1.607]
α	0.786	0.716	0.850	[0.191 - 0.910]
β	0.238	0.249	0.221	[0.121 - 0.435]
γ	0.151	0.162	0.133	[0.086 - 0.301]
η	0.294	0.306	0.267	[0.152 - 0.525]
θ	0.241	0.237	0.277	[0.119 - 0.335]
δ	0.051	0.054	0.032	[0.021 - 0.108]
d	0.140	0.160	0.100	[0.071 - 0.324]

Table S2: Posterior summaries and 95-% credibility intervals for each model parameter recovered from data from the German federal state Bavaria.

	Median	Mean	MAP	95-CI
t_1	7.995	7.906	8.190	[4.424 - 10.887]
t_2	14.757	14.762	14.587	[12.855 - 16.684]
t_3	22.105	22.109	22.039	[20.243 - 23.976]
t_4	65.865	65.849	66.057	[63.599 - 68.034]
Δt_1	3.022	3.156	2.802	[1.623 - 5.450]
Δt_2	2.995	3.105	2.875	[1.695 - 5.116]
Δt_3	2.999	3.121	2.804	[1.667 - 5.260]
Δt_4	2.964	3.097	2.788	[1.589 - 5.366]
λ_0	2.044	2.125	1.897	[1.228 - 3.453]
λ_1	0.550	0.584	0.478	[0.268 - 1.094]
λ_2	0.286	0.298	0.277	[0.146 - 0.515]
λ_3	0.078	0.081	0.073	[0.038 - 0.139]
λ_4	0.155	0.169	0.127	[0.053 - 0.364]
μ	0.107	0.108	0.102	[0.083 - 0.139]
f_I	0.570	0.570	0.573	[0.463 - 0.677]
ϕ_I	0.347	0.347	0.352	[0.056 - 0.637]
f_D	0.432	0.432	0.435	[0.295 - 0.565]
ϕ_D	-0.432	-0.431	-0.433	[-0.683 - -0.171]
D_I	6.686	6.732	6.509	[4.848 - 8.875]
D_D	11.880	11.919	11.914	[9.480 - 14.591]
E_0	16.883	21.504	11.438	[3.499 - 65.947]
σ_I	4.154	4.185	4.078	[3.265 - 5.288]
σ_D	1.218	1.227	1.219	[0.944 - 1.568]
α	0.685	0.620	0.815	[0.106 - 0.887]
β	0.244	0.255	0.223	[0.132 - 0.439]
γ	0.148	0.158	0.129	[0.088 - 0.286]
η	0.296	0.307	0.279	[0.167 - 0.511]
θ	0.219	0.218	0.228	[0.099 - 0.327]
δ	0.050	0.053	0.031	[0.021 - 0.100]
d	0.132	0.153	0.098	[0.071 - 0.317]

Table S3: Posterior summaries and 95-% credibility intervals for each model parameter recovered from data from the German federal state Berlin.

	Median	Mean	MAP	95-CI
t_1	7.580	7.536	7.614	[4.146 - 10.671]
t_2	14.655	14.661	14.509	[12.711 - 16.623]
t_3	21.802	21.807	21.592	[19.849 - 23.786]
t_4	65.489	65.481	65.509	[63.302 - 67.622]
Δt_1	2.935	3.063	2.706	[1.577 - 5.248]
Δt_2	2.880	2.983	2.768	[1.556 - 5.016]
Δt_3	3.049	3.180	2.921	[1.650 - 5.474]
Δt_4	2.963	3.092	2.880	[1.599 - 5.330]
λ_0	1.823	1.900	1.725	[1.045 - 3.201]
λ_1	0.448	0.478	0.382	[0.207 - 0.918]
λ_2	0.222	0.231	0.200	[0.098 - 0.423]
λ_3	0.102	0.104	0.093	[0.052 - 0.173]
λ_4	0.153	0.166	0.135	[0.051 - 0.354]
μ	0.110	0.111	0.106	[0.077 - 0.156]
f_I	0.316	0.316	0.308	[0.209 - 0.423]
ϕ_I	0.276	0.277	0.273	[0.084 - 0.471]
f_D	0.330	0.330	0.333	[0.091 - 0.568]
ϕ_D	-0.141	-0.139	-0.141	[-0.564 - 0.300]
D_I	5.792	5.836	5.637	[4.041 - 7.892]
D_D	15.535	15.591	15.333	[12.276 - 19.240]
E_0	14.154	18.792	9.016	[2.804 - 61.612]
σ_I	1.939	1.955	1.940	[1.520 - 2.477]
σ_D	0.727	0.735	0.717	[0.546 - 0.965]
α	0.688	0.619	0.810	[0.102 - 0.882]
β	0.242	0.254	0.226	[0.127 - 0.446]
γ	0.123	0.133	0.108	[0.070 - 0.255]
η	0.312	0.322	0.287	[0.169 - 0.537]
θ	0.242	0.236	0.282	[0.112 - 0.331]
δ	0.029	0.030	0.024	[0.011 - 0.060]
d	0.129	0.148	0.099	[0.070 - 0.313]

Table S4: Posterior summaries and 95-% credibility intervals for each model parameter recovered from data from the German federal state Brandenburg.

	Median	Mean	MAP	95-CI
t_1	7.550	7.514	7.601	[3.748 - 11.090]
t_2	14.935	14.930	14.918	[12.920 - 16.916]
t_3	22.213	22.215	22.309	[20.315 - 24.155]
t_4	65.019	65.014	65.144	[62.802 - 67.184]
Δt_1	2.907	3.032	2.834	[1.549 - 5.216]
Δt_2	2.972	3.089	2.753	[1.586 - 5.242]
Δt_3	3.298	3.441	3.117	[1.719 - 6.054]
Δt_4	3.028	3.152	2.834	[1.657 - 5.341]
λ_0	2.404	2.537	2.201	[1.272 - 4.553]
λ_1	0.459	0.493	0.415	[0.164 - 1.016]
λ_2	0.379	0.407	0.317	[0.167 - 0.810]
λ_3	0.075	0.080	0.065	[0.023 - 0.158]
λ_4	0.130	0.152	0.103	[0.027 - 0.402]
μ	0.159	0.161	0.155	[0.114 - 0.219]
f_I	0.273	0.273	0.274	[0.109 - 0.439]
ϕ_I	0.375	0.375	0.366	[0.124 - 0.628]
f_D	0.364	0.364	0.377	[0.103 - 0.621]
ϕ_D	0.012	0.012	0.020	[-0.520 - 0.547]
D_I	6.937	6.981	6.816	[4.932 - 9.259]
D_D	15.188	15.249	15.069	[12.053 - 18.808]
E_0	2.853	4.647	1.627	[0.239 - 19.681]
σ_I	2.286	2.308	2.188	[1.763 - 2.971]
σ_D	0.704	0.713	0.674	[0.516 - 0.956]
α	0.843	0.805	0.862	[0.433 - 0.906]
β	0.210	0.220	0.198	[0.092 - 0.405]
γ	0.115	0.124	0.102	[0.066 - 0.233]
η	0.266	0.277	0.244	[0.132 - 0.481]
θ	0.196	0.199	0.176	[0.100 - 0.309]
δ	0.042	0.047	0.030	[0.019 - 0.102]
d	0.168	0.182	0.118	[0.078 - 0.337]

Table S5: Posterior summaries and 95-% credibility intervals for each model parameter recovered from data from the German federal state Bremen.

	Median	Mean	MAP	95-CI
t_1	7.928	7.874	8.182	[3.783 - 11.710]
t_2	14.642	14.643	14.619	[12.640 - 16.647]
t_3	21.816	21.824	21.739	[19.730 - 23.936]
t_4	65.452	65.448	65.313	[63.185 - 67.665]
Δt_1	2.956	3.089	2.737	[1.574 - 5.335]
Δt_2	2.871	2.982	2.679	[1.614 - 4.959]
Δt_3	3.038	3.169	2.751	[1.615 - 5.493]
Δt_4	3.007	3.131	2.813	[1.639 - 5.360]
λ_0	2.122	2.309	1.804	[1.016 - 4.700]
λ_1	0.428	0.486	0.356	[0.118 - 1.185]
λ_2	0.151	0.167	0.122	[0.030 - 0.394]
λ_3	0.189	0.192	0.180	[0.097 - 0.305]
λ_4	0.145	0.162	0.116	[0.031 - 0.391]
μ	0.177	0.179	0.171	[0.121 - 0.253]
f_I	0.379	0.380	0.406	[0.127 - 0.636]
ϕ_I	0.274	0.274	0.271	[-0.148 - 0.695]
f_D	0.651	0.645	0.656	[0.341 - 0.908]
ϕ_D	-1.216	-1.164	-1.373	[-3.460 - 1.374]
D_I	6.654	6.718	6.229	[4.334 - 9.454]
D_D	11.813	11.891	11.852	[8.668 - 15.572]
E_0	2.630	4.397	1.500	[0.161 - 19.437]
σ_I	2.083	2.106	2.039	[1.607 - 2.739]
σ_D	0.547	0.555	0.537	[0.404 - 0.752]
α	0.815	0.748	0.858	[0.219 - 0.914]
β	0.238	0.249	0.228	[0.106 - 0.454]
γ	0.091	0.102	0.076	[0.041 - 0.227]
η	0.281	0.292	0.266	[0.143 - 0.505]
θ	0.205	0.207	0.210	[0.097 - 0.325]
δ	0.035	0.040	0.027	[0.015 - 0.094]
d	0.164	0.175	0.115	[0.072 - 0.320]

Table S6: Posterior summaries and 95-% credibility intervals for each model parameter recovered from data from the German federal state Hamburg.

	Median	Mean	MAP	95-CI
t_1	8.213	8.135	8.422	[4.272 - 11.599]
t_2	14.699	14.705	14.586	[12.721 - 16.726]
t_3	21.796	21.798	21.857	[19.845 - 23.770]
t_4	65.481	65.470	65.606	[63.285 - 67.623]
Δt_1	2.927	3.062	2.672	[1.586 - 5.263]
Δt_2	2.877	2.987	2.754	[1.507 - 5.086]
Δt_3	3.128	3.262	2.901	[1.700 - 5.599]
Δt_4	3.022	3.149	2.837	[1.647 - 5.371]
λ_0	2.266	2.357	2.108	[1.246 - 3.997]
λ_1	0.510	0.568	0.431	[0.189 - 1.287]
λ_2	0.244	0.260	0.232	[0.093 - 0.524]
λ_3	0.086	0.089	0.082	[0.033 - 0.164]
λ_4	0.110	0.124	0.091	[0.022 - 0.311]
μ	0.097	0.098	0.094	[0.065 - 0.140]
f_I	0.557	0.557	0.576	[0.305 - 0.806]
ϕ_I	0.457	0.460	0.506	[-0.222 - 1.165]
f_D	0.447	0.443	0.419	[0.139 - 0.730]
ϕ_D	-0.322	-0.317	-0.339	[-0.997 - 0.389]
D_I	6.064	6.106	5.940	[4.222 - 8.223]
D_D	18.140	18.205	17.825	[14.393 - 22.438]
E_0	3.233	5.171	1.846	[0.259 - 21.555]
σ_I	4.244	4.287	4.123	[3.358 - 5.479]
σ_D	1.290	1.310	1.304	[0.958 - 1.774]
α	0.837	0.788	0.865	[0.342 - 0.910]
β	0.222	0.232	0.203	[0.110 - 0.411]
γ	0.139	0.149	0.128	[0.081 - 0.278]
η	0.298	0.309	0.286	[0.151 - 0.527]
θ	0.251	0.246	0.272	[0.134 - 0.339]
δ	0.043	0.049	0.030	[0.016 - 0.114]
d	0.133	0.155	0.097	[0.067 - 0.323]

Table S7: Posterior summaries and 95-% credibility intervals for each model parameter recovered from data from the German federal state Hesse.

	Median	Mean	MAP	95-CI
t_1	7.500	7.481	7.802	[4.050 - 10.804]
t_2	14.888	14.887	15.080	[12.995 - 16.794]
t_3	21.829	21.839	21.619	[19.881 - 23.852]
t_4	65.325	65.310	65.266	[63.150 - 67.396]
Δt_1	2.972	3.095	2.683	[1.602 - 5.301]
Δt_2	2.918	3.035	2.687	[1.618 - 5.124]
Δt_3	3.140	3.275	2.924	[1.657 - 5.656]
Δt_4	2.939	3.070	2.760	[1.590 - 5.299]
λ_0	2.838	2.997	2.481	[1.494 - 5.423]
λ_1	0.474	0.509	0.420	[0.209 - 1.018]
λ_2	0.234	0.249	0.208	[0.087 - 0.502]
λ_3	0.101	0.104	0.098	[0.049 - 0.173]
λ_4	0.186	0.204	0.156	[0.068 - 0.444]
μ	0.140	0.142	0.135	[0.104 - 0.192]
f_I	0.441	0.441	0.430	[0.251 - 0.629]
ϕ_I	0.460	0.461	0.457	[0.100 - 0.824]
f_D	0.748	0.745	0.752	[0.561 - 0.913]
ϕ_D	-0.743	-0.739	-0.712	[-1.958 - 0.533]
D_I	6.129	6.169	6.060	[4.292 - 8.297]
D_D	13.593	13.646	13.589	[10.946 - 16.686]
E_0	2.141	3.513	1.225	[0.147 - 15.234]
σ_I	4.154	4.192	4.048	[3.257 - 5.329]
σ_D	0.677	0.683	0.669	[0.516 - 0.884]
α	0.797	0.726	0.850	[0.207 - 0.907]
β	0.244	0.255	0.225	[0.125 - 0.443]
γ	0.129	0.140	0.115	[0.070 - 0.274]
η	0.294	0.306	0.273	[0.154 - 0.526]
θ	0.219	0.218	0.236	[0.108 - 0.322]
δ	0.044	0.048	0.031	[0.019 - 0.097]
d	0.150	0.167	0.109	[0.074 - 0.325]

Table S8: Posterior summaries and 95-% credibility intervals for each model parameter recovered from data from the German federal state Lower Saxony.

	Median	Mean	MAP	95-CI
t_1	7.806	7.765	7.607	[4.411 - 10.849]
t_2	14.769	14.769	14.681	[12.874 - 16.668]
t_3	21.712	21.720	21.676	[19.752 - 23.726]
t_4	65.570	65.559	65.628	[63.427 - 67.643]
Δt_1	2.999	3.131	2.709	[1.632 - 5.358]
Δt_2	2.913	3.027	2.717	[1.624 - 5.064]
Δt_3	2.987	3.112	2.710	[1.622 - 5.324]
Δt_4	2.937	3.067	2.776	[1.566 - 5.315]
λ_0	2.623	2.751	2.328	[1.434 - 4.798]
λ_1	0.513	0.552	0.465	[0.230 - 1.100]
λ_2	0.204	0.216	0.188	[0.077 - 0.421]
λ_3	0.113	0.115	0.107	[0.061 - 0.185]
λ_4	0.171	0.184	0.158	[0.065 - 0.383]
μ	0.131	0.133	0.127	[0.094 - 0.182]
f_I	0.562	0.561	0.558	[0.396 - 0.725]
ϕ_I	0.125	0.125	0.123	[-0.277 - 0.534]
f_D	0.461	0.458	0.465	[0.230 - 0.674]
ϕ_D	-0.016	-0.016	-0.012	[-0.523 - 0.487]
D_I	6.031	6.071	6.130	[4.233 - 8.135]
D_D	13.852	13.914	13.922	[11.073 - 17.083]
E_0	2.776	4.328	1.587	[0.216 - 17.888]
σ_I	3.411	3.437	3.404	[2.688 - 4.336]
σ_D	1.104	1.114	1.112	[0.839 - 1.452]
α	0.767	0.691	0.841	[0.157 - 0.901]
β	0.245	0.256	0.227	[0.128 - 0.441]
γ	0.136	0.147	0.120	[0.076 - 0.284]
η	0.319	0.330	0.284	[0.176 - 0.548]
θ	0.239	0.235	0.259	[0.117 - 0.332]
δ	0.057	0.062	0.038	[0.024 - 0.131]
d	0.146	0.164	0.102	[0.069 - 0.327]

Table S9: Posterior summaries and 95-% credibility intervals for each model parameter recovered from data from the German federal state Mecklenburg-Western Pomerania.

	Median	Mean	MAP	95-CI
t_1	7.525	7.471	7.622	[3.152 - 11.459]
t_2	14.807	14.809	14.761	[12.897 - 16.727]
t_3	21.557	21.565	21.635	[19.656 - 23.503]
t_4	65.753	65.748	65.729	[63.662 - 67.819]
Δt_1	2.957	3.080	2.718	[1.598 - 5.256]
Δt_2	2.960	3.070	2.758	[1.650 - 5.080]
Δt_3	2.776	2.894	2.504	[1.498 - 4.989]
Δt_4	2.973	3.090	2.760	[1.579 - 5.263]
λ_0	1.403	1.457	1.330	[0.801 - 2.441]
λ_1	0.479	0.502	0.444	[0.226 - 0.914]
λ_2	0.213	0.226	0.192	[0.077 - 0.453]
λ_3	0.099	0.102	0.095	[0.055 - 0.161]
λ_4	0.187	0.200	0.157	[0.067 - 0.410]
μ	0.124	0.126	0.117	[0.086 - 0.177]
f_I	0.416	0.416	0.419	[0.159 - 0.668]
ϕ_I	0.324	0.324	0.326	[-0.153 - 0.802]
f_D	0.701	0.693	0.721	[0.382 - 0.952]
ϕ_D	-0.464	-0.453	-0.701	[-3.852 - 3.016]
D_I	6.238	6.282	6.101	[4.411 - 8.409]
D_D	12.285	12.354	11.986	[9.076 - 16.036]
E_0	2.103	3.357	1.219	[0.138 - 14.299]
σ_I	1.706	1.726	1.635	[1.316 - 2.253]
σ_D	0.456	0.465	0.448	[0.332 - 0.646]
α	0.738	0.659	0.831	[0.127 - 0.896]
β	0.257	0.268	0.234	[0.141 - 0.457]
γ	0.179	0.194	0.162	[0.108 - 0.370]
η	0.354	0.362	0.331	[0.188 - 0.588]
θ	0.285	0.274	0.306	[0.143 - 0.341]
δ	0.015	0.017	0.013	[0.005 - 0.037]
d	0.119	0.132	0.092	[0.062 - 0.274]

Table S10: Posterior summaries and 95-% credibility intervals for each model parameter recovered from data from the German federal state North Rhine-Westphalia.

	Median	Mean	MAP	95-CI
t_1	5.485	5.476	5.442	[2.224 - 8.708]
t_2	14.797	14.796	14.884	[12.896 - 16.693]
t_3	21.778	21.788	21.717	[19.868 - 23.775]
t_4	65.723	65.712	65.657	[63.437 - 67.929]
Δt_1	2.906	3.022	2.687	[1.575 - 5.116]
Δt_2	2.952	3.062	2.772	[1.640 - 5.099]
Δt_3	3.123	3.251	2.808	[1.671 - 5.539]
Δt_4	2.941	3.068	2.771	[1.575 - 5.309]
λ_0	2.628	2.791	2.265	[1.434 - 5.074]
λ_1	0.465	0.483	0.436	[0.242 - 0.836]
λ_2	0.261	0.276	0.238	[0.109 - 0.530]
λ_3	0.093	0.096	0.089	[0.048 - 0.160]
λ_4	0.188	0.204	0.162	[0.070 - 0.432]
μ	0.137	0.139	0.136	[0.102 - 0.188]
f_I	0.670	0.669	0.667	[0.495 - 0.841]
ϕ_I	0.164	0.164	0.166	[-0.456 - 0.773]
f_D	0.522	0.520	0.528	[0.320 - 0.710]
ϕ_D	-0.603	-0.598	-0.600	[-1.069 - -0.097]
D_I	5.741	5.785	5.598	[4.005 - 7.783]
D_D	14.037	14.087	13.964	[11.269 - 17.202]
E_0	10.213	14.590	6.165	[1.164 - 54.135]
σ_I	6.285	6.338	6.197	[4.968 - 8.023]
σ_D	1.440	1.451	1.413	[1.107 - 1.859]
α	0.719	0.647	0.830	[0.117 - 0.900]
β	0.248	0.259	0.230	[0.127 - 0.453]
γ	0.141	0.153	0.119	[0.078 - 0.293]
η	0.290	0.302	0.264	[0.159 - 0.516]
θ	0.209	0.211	0.194	[0.100 - 0.323]
δ	0.050	0.054	0.034	[0.022 - 0.108]
d	0.151	0.168	0.106	[0.074 - 0.326]

Table S11: Posterior summaries and 95-% credibility intervals for each model parameter recovered from data from the German federal state Rhineland-Palatinate.

	Median	Mean	MAP	95-CI
t_1	6.170	6.178	6.122	[3.256 - 9.143]
t_2	14.752	14.746	14.668	[12.827 - 16.655]
t_3	21.926	21.932	21.983	[20.003 - 23.906]
t_4	65.349	65.340	65.402	[63.171 - 67.468]
Δt_1	2.887	3.004	2.710	[1.575 - 5.086]
Δt_2	2.975	3.089	2.776	[1.639 - 5.184]
Δt_3	3.138	3.274	2.796	[1.679 - 5.644]
Δt_4	2.970	3.099	2.729	[1.634 - 5.286]
λ_0	2.902	3.042	2.780	[1.594 - 5.255]
λ_1	0.366	0.381	0.344	[0.185 - 0.667]
λ_2	0.241	0.252	0.215	[0.109 - 0.465]
λ_3	0.086	0.088	0.079	[0.040 - 0.152]
λ_4	0.186	0.202	0.163	[0.073 - 0.423]
μ	0.107	0.109	0.105	[0.076 - 0.150]
f_I	0.747	0.747	0.750	[0.561 - 0.929]
ϕ_I	0.344	0.347	0.382	[-0.656 - 1.388]
f_D	0.750	0.745	0.738	[0.506 - 0.951]
ϕ_D	-0.601	-0.586	-0.557	[-2.984 - 1.894]
D_I	6.205	6.245	6.149	[4.424 - 8.290]
D_D	14.018	14.068	13.659	[11.035 - 17.385]
E_0	2.516	4.058	1.462	[0.195 - 17.231]
σ_I	2.632	2.650	2.573	[2.091 - 3.323]
σ_D	0.931	0.940	0.928	[0.708 - 1.228]
α	0.808	0.739	0.858	[0.219 - 0.915]
β	0.242	0.252	0.221	[0.128 - 0.435]
γ	0.131	0.141	0.119	[0.077 - 0.260]
η	0.305	0.315	0.268	[0.156 - 0.534]
θ	0.241	0.236	0.254	[0.125 - 0.326]
δ	0.032	0.034	0.025	[0.013 - 0.068]
d	0.130	0.149	0.099	[0.070 - 0.314]

Table S12: Posterior summaries and 95-% credibility intervals for each model parameter recovered from data from the German federal state Saarland.

	Median	Mean	MAP	95-CI
t_1	8.536	8.395	8.852	[3.429 - 12.561]
t_2	14.925	14.927	14.973	[12.937 - 16.943]
t_3	22.320	22.323	22.372	[20.486 - 24.186]
t_4	65.725	65.716	65.663	[63.536 - 67.859]
Δt_1	2.992	3.116	2.994	[1.604 - 5.345]
Δt_2	3.003	3.127	2.739	[1.617 - 5.333]
Δt_3	3.032	3.154	2.832	[1.634 - 5.380]
Δt_4	3.053	3.181	2.787	[1.638 - 5.459]
λ_0	1.680	1.736	1.579	[0.918 - 2.872]
λ_1	0.717	0.769	0.655	[0.249 - 1.584]
λ_2	0.446	0.472	0.405	[0.187 - 0.903]
λ_3	0.061	0.064	0.057	[0.022 - 0.123]
λ_4	0.129	0.146	0.106	[0.031 - 0.361]
μ	0.122	0.124	0.120	[0.088 - 0.171]
f_I	0.571	0.571	0.568	[0.291 - 0.849]
ϕ_I	0.426	0.430	0.430	[-0.461 - 1.332]
f_D	0.658	0.649	0.697	[0.345 - 0.900]
ϕ_D	-0.175	-0.174	-0.213	[-1.940 - 1.612]
D_I	7.371	7.410	7.343	[5.281 - 9.787]
D_D	14.582	14.639	14.307	[11.376 - 18.221]
E_0	1.441	2.294	0.793	[0.085 - 9.603]
σ_I	3.512	3.555	3.473	[2.720 - 4.624]
σ_D	1.029	1.045	1.006	[0.768 - 1.417]
α	0.851	0.808	0.873	[0.392 - 0.935]
β	0.225	0.235	0.210	[0.112 - 0.415]
γ	0.179	0.191	0.161	[0.112 - 0.345]
η	0.287	0.298	0.262	[0.149 - 0.505]
θ	0.247	0.243	0.276	[0.131 - 0.332]
δ	0.050	0.057	0.034	[0.019 - 0.135]
d	0.147	0.165	0.102	[0.069 - 0.325]

Table S13: Posterior summaries and 95-% credibility intervals for each model parameter recovered from data from the German federal state Saxony-Anhalt.

	Median	Mean	MAP	95-CI
t_1	7.024	7.014	7.331	[3.248 - 10.697]
t_2	14.713	14.715	14.820	[12.786 - 16.657]
t_3	21.826	21.839	21.710	[19.889 - 23.844]
t_4	66.066	66.066	65.894	[63.906 - 68.196]
Δt_1	2.940	3.059	2.683	[1.581 - 5.202]
Δt_2	2.912	3.018	2.711	[1.591 - 5.035]
Δt_3	3.094	3.230	2.960	[1.670 - 5.519]
Δt_4	3.008	3.129	2.979	[1.672 - 5.289]
λ_0	2.404	2.531	2.254	[1.291 - 4.470]
λ_1	0.464	0.492	0.420	[0.200 - 0.949]
λ_2	0.233	0.248	0.218	[0.091 - 0.499]
λ_3	0.091	0.094	0.078	[0.034 - 0.169]
λ_4	0.126	0.138	0.110	[0.037 - 0.315]
μ	0.122	0.124	0.118	[0.085 - 0.173]
f_I	0.617	0.617	0.636	[0.349 - 0.881]
ϕ_I	-0.285	-0.283	-0.235	[-1.326 - 0.781]
f_D	0.684	0.674	0.699	[0.356 - 0.938]
ϕ_D	-0.930	-0.891	-1.023	[-3.366 - 1.788]
D_I	6.706	6.758	6.549	[4.793 - 8.986]
D_D	12.185	12.244	12.030	[9.133 - 15.714]
E_0	1.720	3.003	0.974	[0.089 - 13.726]
σ_I	2.422	2.447	2.443	[1.895 - 3.156]
σ_D	0.800	0.812	0.794	[0.598 - 1.093]
α	0.853	0.808	0.878	[0.374 - 0.944]
β	0.229	0.239	0.203	[0.112 - 0.423]
γ	0.132	0.142	0.121	[0.076 - 0.269]
η	0.294	0.305	0.282	[0.145 - 0.525]
θ	0.267	0.260	0.287	[0.148 - 0.339]
δ	0.026	0.028	0.020	[0.010 - 0.063]
d	0.136	0.154	0.100	[0.070 - 0.313]

Table S14: Posterior summaries and 95-% credibility intervals for each model parameter recovered from data from the German federal state Saxony.

	Median	Mean	MAP	95-CI
t_1	8.342	8.284	8.347	[4.622 - 11.562]
t_2	14.719	14.720	14.756	[12.803 - 16.658]
t_3	21.814	21.822	21.738	[19.872 - 23.808]
t_4	65.651	65.645	65.754	[63.545 - 67.726]
Δt_1	3.005	3.140	2.872	[1.638 - 5.381]
Δt_2	2.912	3.029	2.652	[1.595 - 5.087]
Δt_3	2.976	3.098	2.875	[1.650 - 5.235]
Δt_4	2.975	3.101	2.737	[1.607 - 5.330]
λ_0	2.460	2.568	2.267	[1.343 - 4.400]
λ_1	0.509	0.558	0.454	[0.199 - 1.219]
λ_2	0.216	0.228	0.213	[0.087 - 0.441]
λ_3	0.101	0.104	0.093	[0.052 - 0.171]
λ_4	0.164	0.178	0.138	[0.056 - 0.379]
μ	0.115	0.117	0.112	[0.082 - 0.160]
f_I	0.683	0.683	0.688	[0.472 - 0.891]
ϕ_I	0.467	0.471	0.444	[-0.426 - 1.391]
f_D	0.569	0.564	0.571	[0.281 - 0.822]
ϕ_D	-0.175	-0.171	-0.186	[-1.130 - 0.804]
D_I	6.506	6.553	6.387	[4.623 - 8.722]
D_D	13.650	13.702	13.310	[10.663 - 17.066]
E_0	1.676	2.718	0.977	[0.093 - 11.765]
σ_I	2.850	2.874	2.776	[2.261 - 3.626]
σ_D	0.861	0.870	0.831	[0.651 - 1.143]
α	0.810	0.741	0.862	[0.225 - 0.919]
β	0.244	0.255	0.232	[0.130 - 0.437]
γ	0.138	0.149	0.121	[0.080 - 0.283]
η	0.321	0.332	0.310	[0.172 - 0.548]
θ	0.250	0.245	0.249	[0.129 - 0.336]
δ	0.038	0.041	0.026	[0.015 - 0.086]
d	0.134	0.153	0.095	[0.067 - 0.319]

Table S15: Posterior summaries and 95-% credibility intervals for each model parameter recovered from data from the German federal state Schleswig-Holstein.

	Median	Mean	MAP	95-CI
t_1	7.984	7.893	8.296	[3.788 - 11.495]
t_2	14.775	14.778	14.788	[12.870 - 16.709]
t_3	21.842	21.853	21.840	[19.896 - 23.865]
t_4	65.779	65.771	65.984	[63.619 - 67.891]
Δt_1	2.987	3.116	2.693	[1.602 - 5.350]
Δt_2	2.914	3.028	2.653	[1.572 - 5.123]
Δt_3	3.088	3.218	2.991	[1.680 - 5.500]
Δt_4	2.990	3.116	2.774	[1.649 - 5.319]
λ_0	2.038	2.134	1.812	[1.112 - 3.721]
λ_1	0.552	0.595	0.469	[0.217 - 1.227]
λ_2	0.240	0.254	0.214	[0.097 - 0.499]
λ_3	0.087	0.090	0.077	[0.037 - 0.161]
λ_4	0.139	0.154	0.109	[0.039 - 0.359]
μ	0.122	0.124	0.118	[0.089 - 0.169]
f_I	0.412	0.412	0.408	[0.218 - 0.603]
ϕ_I	0.132	0.132	0.137	[-0.228 - 0.496]
f_D	0.484	0.481	0.491	[0.212 - 0.736]
ϕ_D	-0.925	-0.920	-0.923	[-1.613 - -0.197]
D_I	6.575	6.625	6.355	[4.650 - 8.866]
D_D	13.320	13.380	13.245	[10.391 - 16.730]
E_0	4.041	6.161	2.337	[0.410 - 24.373]
σ_I	2.287	2.307	2.255	[1.794 - 2.929]
σ_D	0.633	0.640	0.623	[0.478 - 0.838]
α	0.799	0.733	0.844	[0.222 - 0.896]
β	0.239	0.250	0.228	[0.122 - 0.439]
γ	0.128	0.139	0.114	[0.075 - 0.261]
η	0.286	0.297	0.269	[0.147 - 0.504]
θ	0.247	0.241	0.280	[0.124 - 0.332]
δ	0.042	0.045	0.028	[0.017 - 0.094]
d	0.140	0.159	0.101	[0.070 - 0.323]

Table S16: Posterior summaries and 95-% credibility intervals for each model parameter recovered from data from the German federal state Thuringia.

	Median	Mean	MAP	95-CI
t_1	8.751	8.645	8.705	[4.418 - 12.199]
t_2	14.716	14.722	14.742	[12.787 - 16.691]
t_3	21.773	21.779	21.833	[19.729 - 23.869]
t_4	65.537	65.532	65.699	[63.380 - 67.635]
Δt_1	2.975	3.107	2.733	[1.603 - 5.324]
Δt_2	2.868	2.981	2.666	[1.541 - 5.084]
Δt_3	3.138	3.276	2.990	[1.699 - 5.680]
Δt_4	3.016	3.143	2.870	[1.669 - 5.331]
λ_0	2.237	2.381	1.957	[1.148 - 4.482]
λ_1	0.551	0.623	0.426	[0.156 - 1.508]
λ_2	0.214	0.229	0.191	[0.079 - 0.469]
λ_3	0.135	0.139	0.128	[0.067 - 0.228]
λ_4	0.115	0.126	0.097	[0.026 - 0.296]
μ	0.108	0.109	0.102	[0.072 - 0.157]
f_I	0.431	0.431	0.430	[0.242 - 0.617]
ϕ_I	0.068	0.068	0.062	[-0.285 - 0.431]
f_D	0.380	0.378	0.388	[0.105 - 0.643]
ϕ_D	-0.671	-0.665	-0.697	[-1.188 - -0.098]
D_I	6.517	6.565	6.192	[4.493 - 8.908]
D_D	15.128	15.191	15.156	[11.714 - 19.041]
E_0	2.087	3.433	1.215	[0.140 - 14.945]
σ_I	2.109	2.126	2.070	[1.641 - 2.711]
σ_D	0.857	0.867	0.853	[0.641 - 1.150]
α	0.837	0.785	0.862	[0.323 - 0.912]
β	0.232	0.243	0.217	[0.115 - 0.434]
γ	0.114	0.125	0.097	[0.057 - 0.255]
η	0.293	0.304	0.272	[0.150 - 0.517]
θ	0.207	0.209	0.207	[0.102 - 0.320]
δ	0.058	0.065	0.037	[0.023 - 0.145]
d	0.143	0.162	0.098	[0.067 - 0.326]